# Influence of a neighbouring Cu centre on electro- and photocatalytic $CO_2$ reduction by Fe-Mabiq

*Kerstin Rickmeyer, Matthias Huber, Corinna R. Hess**

Department of Chemistry and Catalysis Research Center (CRC), Technical University of Munich, Lichtenbergstr. 4, 85748 Garching, Germany; Faculty of Chemistry and Pharmacy, University of Regensburg, 93053 Regensburg, Germany

**Corresponding Author**

*corinna.hess@ch.tum.de

**17 April 2024**

**Note added after first publication:** This supplementary information file replaces that originally published on 14 December 2023. Some incorrect values related to product formation were reported in Table S5, S6 and S7. The data in these tables have now been corrected, along with the corresponding y-axis values in Figure S15, S16, S19 and S20.

**Table of Contents**


General ..... 3
Instrumentation ..... 3
Crystallography ..... 8
Synthesis ..... 9
$^{1}$H-, $^{31}$P- and $^{19}$F-NMR of **1**, **2** and **3** ..... 11
Comparison of $^{1}$H-NMR of **1**, **2** and **3** in the aromatic region ..... 17
Molecular structure of **2** ..... 18
Absorption spectra of **1** and **2** ..... 23
IR spectra of **1** and **2** ..... 23
CV data for **1** and **2** ..... 25
[PhOH] dependence of **2** ..... 25
Headspace analysis after photocatalysis experiments ..... 25
NMR of precipitate after photocatalysis ..... 29
Concentration dependence for photocatalytic $CO_2$ reduction ..... 30
Proton source dependence for photocatalytic $CO_2$ reduction by **1** and **2** ..... 31
CV of **1** and **2** in the presence of $H_2O$ and $CO_2$ ..... 33
Quantum Yield Determination experiments for the photoreduction of **1** and **2** ..... 35
Molecular structure of **1** ..... 39
References ..... 43

## General

All chemicals were purchased from Sigma Aldrich and used without further purification unless noted otherwise. Metal compounds were synthesized in an inert atmosphere glove box (Ar), using anhydrous solvents. Dry solvents were obtained from an MBraun SPS, deoxygenated via freeze-pump-thaw cycles and stored over 3 Å (MeCN, Pentane) or 4 Å activated molecular sieves. Tetrabutylammonium hexafluorophosphate ($[N(n\text{-}Bu)_4]PF_6$) was recrystallized three times from ethanol,[1] and ferrocene was sublimed prior to use. Dry $CD_3CN$ was purchased from Sigma Aldrich, deoxygenated by the freeze-pump-thaw method, stored over 3 Å molecular sieves and filtered over activated aluminum oxide prior to use (activated, standard grade, neutral, Brokmann I, 58 Å pore size). Carbon dioxide (5.0 purity, Westfahlen AG, Münster, Germany) was passed through a 3 Å molecular sieve drying column to remove trace water.[2]

## Instrumentation

Electronic spectra were measured on an Agilent Cary 60 UV-Vis spectrophotometer.

Solution state NMR spectra were measured on a Bruker Avance Ultrashield (400 MHz $^{1}H$, 162 MHz $^{31}P$) or a Bruker Avance HD (376 MHz $^{19}F$) spectrometer with Topspin 2.1 software. The data was analyzed using MestreNova (Mestrelab Research S.L.). The following abbreviations were used: s = singlet, d = doublet, m = multiplet, dd = doublet of doublets, ddd = doublet of doublet of doublets.

Electrospray Ionisation mass spectrometry (ESI-MS) was performed using a Thermo Scientific Exactive Plus Benchtop LC-MS equipped with a Thermo Scientific Orbitrap Mass Analyzer. THF was used as a solvent, unless noted otherwise.

Elemental analysis was carried out at the Technical University of Munich.

Cyclic Voltammetry was carried out with a BioLogic SP200 potentiostat with EC-Lab software, using 3 mm diameter glassy carbon disk electrodes (PalmSens, Houten Netherlands) as working and counter electrodes. Prior to use, electrodes were polished with 0.05 µm alumina suspensions (CH Instruments Inc., USA). $Ag/AgNO_3$ (10 mM $AgNO_3$ and 0.1 M $[N(n\text{-}Bu)_4]PF_6$ in MeCN) was used as the reference electrode, separated via a Vycor 3535 frit (Advanced Glass & Ceramics, Holden, MA). CV measurements were performed in a five-necked glass cell under an Ar atmosphere. For measurements under $CO_2$ atmosphere, the solution was purged for 5 min and the cell was kept under that atmosphere during the experiment. Unless noted otherwise, a scan rate of 100 mV/s was applied. Potentials are reported with reference to an internal standard of ferrocenium/ferrocene ($Fc^{+/0}$, given by $V_{Fc}$).

Photocatalytic experiments were carried out in crimp glass vials with a total volume of 8.5 mL. Dry and deoxygenated MeCN was used as solvent for all experiments except for experiments with $^{13}CO_2$ where $CD_3CN$ was used instead to allow for direct measurement of the liquid phase in the NMR. In a standard experiment 100 mM of BIH as sacrificial electron donor, 200 µM of $[Ru(bpy)_3](PF_6)_2$ as photosensitizer, 2 µM of catalyst and 85 equiv. of PhOH in a total volume of 2 mL were added to the vial in the glove box under red light. The vials were sealed and the solution was purged with $CO_2$ for 2 min followed by irradiation at 455 nm for 1 h using our previously reported photoreactor.[3, 4] A constant temperature of 20 °C was ensured by cooling with running water. At the end of the irradiation a head space sample was taken using a gastight syringe and analyzed by gas chromatography (GC).

Head space analysis was performed by injecting the gaseous sample directly into the GC (SRI 8610C Gas Chromatograph) and analyzed using a thermal conductivity (TCD) and a flame ionization detector equipped with a methanizer (FID-M). The detectors were calibrated using standard gas mixtures of CO in $N_2$ (AirProducts) and dilutions of $H_2$ or CO in $N_2$, respectively. In order to quantify the amount of gaseous product ($H_2$ or CO) produced, the headspace volume of the cell was determined. The amount of gaseous product generated in the reaction ($n_{prod,gas}$) was calculated as follows:

$$n_{prod,gas} = \frac{x_{prod,gas} \times V_h}{V_M} \quad (1)$$

where $x_{prod,gas}$ is the measured amount of gaseous product in ppm, $V_h = 6.52\,mL$ is the headspace volume of the cell, and $V_M = 24.471\,\frac{L}{mol}$ describes the molar volume. All experiments were carried out in at least triplicate. To account for gaseous products in solution Henry's law was applied.[5] The partial pressure at the end of the experiment ($p_{gas}$) was determined according to equation (2), with the ideal gas constant $R = 8.314\,\frac{J}{K*mol}$ and the temperature $T = 298\,K$.

$$p_{gas} = \frac{n_{prod,gas} \times R \times T}{V_h} \quad (2)$$

The amount of gaseous product in solution ($n_{prod,solv}$) can then be determined as follows:

$$n_{prod,solv} = x_{prod,solv} \times n_{MeCN} = \frac{p_{gas} \times \rho_{MeCN} \times V_{MeCN}}{K_{H,gas} \times M_{MeCN}} \quad (3)$$

where $x_{prod,solv}$ is the mole fraction of dissolved gaseous product, $n_{MeCN}$ is the amount of solvent (MeCN) in [mol], $\rho_{MeCN} = 0.786\,\frac{g}{mL}$ is the density of MeCN, $V_{MeCN} = 2\,mL$ is the

reaction volume, $M_{MeCN} = 41.05\ \frac{g}{mol}$ is the molecular weight of MeCN and $K_{H,gas}$ is the Henry constant with $K_{H,CO} = 2507\ \frac{bar*mol_{MeCN}}{mol_{CO}}$ for CO in MeCN and $K_{H,H_2} = 5618\ \frac{bar*mol_{MeCN}}{mol_{H_2}}$ for $H_2$ in MeCN.[5, 6] The total amount of gaseous product formed ($n_{prod,total}$) is then:

$$n_{prod,total} = n_{prod,gas} + n_{prod,solv} \tag{4}$$

The turn-over number (TON) corresponding to the headspace sample taken at the end of the reaction was calculated according to equation (5), where $n_{catalyst}$ represents the amount of catalyst in [mol] used for the experiment and $n_{prod,total}$ being the total amount of gaseous product produced:

$$TON = \frac{n_{prod,total}}{n_{catalyst}} \tag{5}$$

The TOF in [$s^{-1}$] was obtained by equation (6) where $t$ is the overall time of the reaction in [s]:

$$TOF = \frac{TON}{t} \tag{6}$$

Mass spectrometry of gaseous samples was performed using a Hiden HPR-20 QIC Benchtop Gas Analysis System equipped with a Secondary Electron Multiplier (SEM) detector.

Quantum yield determination measurements were carried out using our Quantum Yield Determination Set-up (QYDS) as previously described.[3, 4, 7] The components are contained within a black box to protect the sample from any external light sources and the experimenter from the intense stray light. A high-power LED ($\lambda_{exc}$ = 455 nm) of type LD-CQ7P-1U3U produced by Osram was used as the excitation light source. The current for the LED was

controlled by a power supply of type RND 320-KA3005P from RND lab. The lens system consists of a Thorlabs aspheric condenser lens (f = 32 mm, 50 mm diameter) and a Thorlabs plano-convex lens (f = 100 mm, 50 mm diameter). The light bundle was imaged through an aperture (8 mm × 8 mm square) in front of the cuvette holder and onto the middle of the cuvette. A shutter was placed between the lens system and the aperture to interrupt the incoming light beam during the measurement, as warranted. The 10 mm × 10 mm fused silica sample cuvette was fitted with a ChemGlass valve. The volume of the sample solutions was 2 mL. During the irradiation period the solutions were rigorously stirred. The transmitted light power of the sample solution ($P_{sample}$) was detected using a Thorlabs power meter of type S175C. To determine the reference power ($P_{ref}$) a cuvette containing 2 mL of solvent was irradiated using the same input power settings as for the sample before each experiment. The incoming light beam was interrupted via a shutter control box, at which point the timer was also paused. The cuvette was subsequently transferred to the Cary60 UV-Vis instrument and the absorption spectrum was recorded. The cuvette was placed back into the QYDS and the illumination was continued. The quantum yield is given by the amount of product formed divided by the number of absorbed photons.[4, 8] The number of absorbed photons was calculated from the difference of the reference power and the power reaching the photometer.[4] To determine the amount of product formed the absorption at two different wavelengths was monitored.

Infrared (IR) spectroscopy was performed in an Ar-filled glove box with a Bruker ALPHA FT-IR spectrometer with Opus/Mentor software equipped with a PLATINUM-ATR unit for analysis of solid samples. Solution IR was carried out at a concentration of 6 mM in MeCN using a LIQUID CELL A145.

**Crystallography**

Crystallographic data were collected on an X-Ray single crystal diffractometer equipped with a TXS rotating anode with MoKα radiation (λ = 0.71073 Å), a CMOS detector (Apex IV, κ-CMOS) and a Helios optic using the Apex IV software package.[9] The measurements were performed on single crystals overlaid with perfluorinated ether. A suitable crystal was transferred to the diffractometer on top of a kapton micro sampler. The measurements were carried out at 100 K using a nitrogen stream. Initial lattice parameters were determined by a matrix scan. Reflections were corrected for Lorentz and polarization effects, scan speed, and background using SAINT.[10] Absorption corrections, including odd and even ordered spherical harmonics were performed using SADABS.[10] Space group assignments were based upon systematic absences, E statistics, and successful refinement of the structures. Structures were solved by SHELXT[11] with the aid of successive difference Fourier maps, and were refined against all data using SHELXL-2018[12] in conjunction with SHELXLE.[13] Hydrogen atoms were assigned to ideal positions and refined using a riding model with an isotropic thermal parameter 1.2 times that of the attached carbon atom (1.5 times for methyl hydrogen atoms). If not mentioned otherwise, non-hydrogen atoms were refined with anisotropic displacement parameters. Full-matrix least squares refinements were carried out by minimizing $\sum w({F_o}^2 - {F_c}^2)^2$ with the SHELXL[12] weighting scheme. Neutral atom scattering factors for all atoms and anomalous dispersion corrections for the non-hydrogen atoms were taken from International Tables for Crystallography.[14] Disordered solvent molecules were treated as a diffuse contribution to the overall scattering without specific atoms positions using the PLATON/SQUEEZE procedure.[15] For **1**, overall 156 electrons corresponding to 1.75 residual MeCN molecules and for **2**, overall 183 electrons corresponding to 2 residual diethylether molecules were determined. Images of the

crystal structures were generated using Mercury.[16] CCDC 2284733-2284734 contains the supplementary crystallographic data for this paper.

**Synthesis**

1,3-dimethyl-2-phenyl-2,3-dihydro-1H-benzo[d]imidazole (BIH) was synthesized according to literature procedures.[17, 18] HMabiq and [Zn(Mabiq)(OTf)] (**4**) were synthesized as previously described.[4, 19]

[Fe(Mabiq)(MeCN)$_2$]OTf (**1**) was synthesized according to a modified literature procedure[20] by adding a solution of Fe(OTf)$_2$ (65.2 mg, 184.3 µmol) in MeCN to a mixture of HMabiq (100 mg, 184.3 µmol) and triethylamine (25.7 µL, 184.3 µmol) in MeCN, leading to an immediate color change to intense green. The mixture was stirred overnight to ensure complete complexation. The solution was filtered through celite, dried and recrystallized from MeCN/Et$_2$O yielding **1** (98.3 mg, 125 µmol, 67.7%).

$^1$H-NMR (400 MHz, CD$_3$CN): δ (ppm) = 9.24 (dd, J = 8.2, 1.5 Hz, 2H), 8.33 (d, J = 8.3 Hz, 2H), 8.11 (ddd, J = 8.3, 6.9, 1.5 Hz, 2H), 7.95 (ddd, J = 8.1, 6.9, 1.2 Hz, 2H), 7.01 (s, 1H), 1.96 (s, 6H), 1.53 (s, 24H). $^{19}$F-NMR (376 MHz, THF-d$_8$): δ (ppm) = 77.74. Elemental analysis calcd. (%) for $C_{38}H_{39}F_3FeN_{10}O_3S$: C, 55.08, H, 4.74, N, 16.90, S, 3.87 found C, 54.73, H, 4.51, N, 16.70, S, 3.61. UV-Vis [$\lambda_{max}$, nm (ε, $10^3$ $M^{-1}cm^{-1}$), in MeCN]: 310 (29.4), 322 (24.4), 351 (44.5), 437 (12.3), 464 (14.8), 630 (5.8), 665 (6.1).

[Cu(Xantphos)Fe(Mabiq)(MeCN)(OTf)]OTf (**2**) was synthesized by adding a solution of **3** (*vide infra*) (19.1 mg, 24.13 µmol) in THF to **1** (20.0 mg, 24.13 µmol) in THF leading to a color

change from green to brown. The solution was stirred for 30 min, filtered through celite, dried and recrystallized from THF/Pentane to give **2** (38.1 mg, 24.13 µmol, 100%). Under these conditions, both NMR and elemental analysis indicate one MeCN coordinated to the Fe center. These samples were used in all catalytic experiments. Single crystals suitable for XRD were obtained from DCM/$Et_2O$; the corresponding structure shows both triflate anions coordinated to the Fe center instead of MeCN (i.e., [Cu(Xantphos)Fe(Mabiq)$(OTf)_2$]).

$^1$H-NMR (400 MHz, THF-$d_8$): δ (ppm) = 9.60 (d, *J* = 8.1 Hz, 2H), 8.40 (s, 2H), 7.86 (d, *J* = 7.7 Hz, 2H), 7.38–6.89 (m, 27H), 6.36 (m, 2H), 1.99 (s, 6H), 1.88 (s, 3H), 1.60 (s, 12H), 1.17 (s, 12H). $^{31}$P-NMR (162 MHz, THF-$d_8$): δ (ppm) = 11.05. $^{19}$F-NMR (376 MHz, THF-$d_8$): δ (ppm) = 76.26. Elemental analysis calcd. (%) for $C_{76}H_{68}CuF_6FeN_9O_7P_2S_2$: C, 57.82, H, 4.34, N, 7.98, S, 4.06 found C, 57.64, H, 4.34, N, 7.55, S, 3.91. UV-Vis [$\lambda_{max}$, nm (ε, $10^3$ $M^{-1}cm^{-1}$), in MeCN]: 310 (34.6), 322 (37.5), 351 (47.65), 437 (13.45), 464 (16.2), 630 (6.15), 665 (6.5).

[Cu(Xantphos)(OTf)] (**3**) was obtained by addition of a solution of [Cu$(MeCN)_4$]OTf (65.1 mg, 172.8 µmol) in THF to 1 equiv. of Xantphos (100 mg, 172.8 µmol). The mixture was stirred for 30 min, filtered through celite and dried, followed by recrystallization from THF/Pentane to give **3** in 100% yield (136.7 mg, 172.8 µmol).

$^1$H-NMR (400 MHz, $CDCl_3$): δ (ppm) = 7.58 (d, *J* = 7.8 Hz, 2H), 7.34 (m, 10H), 7.25 (m, 10H), 7.14 (dd, *J* = 8.8, 6.5 Hz, 2H), 6.65 (m, 2H), 1.68 (s, 6H). $^{31}$P-NMR (162 MHz, $CDCl_3$): δ (ppm) = 15.58. $^{19}$F-NMR (376 MHz, $CDCl_3$): δ (ppm) = 77.59. ESI-MS: [Cu(Xantphos)]$^+$ (*m*/*z*: 641.1212, calc. 641.1219).

## $^{1}$H-, $^{31}$P- and $^{19}$F-NMR of 1, 2 and 3

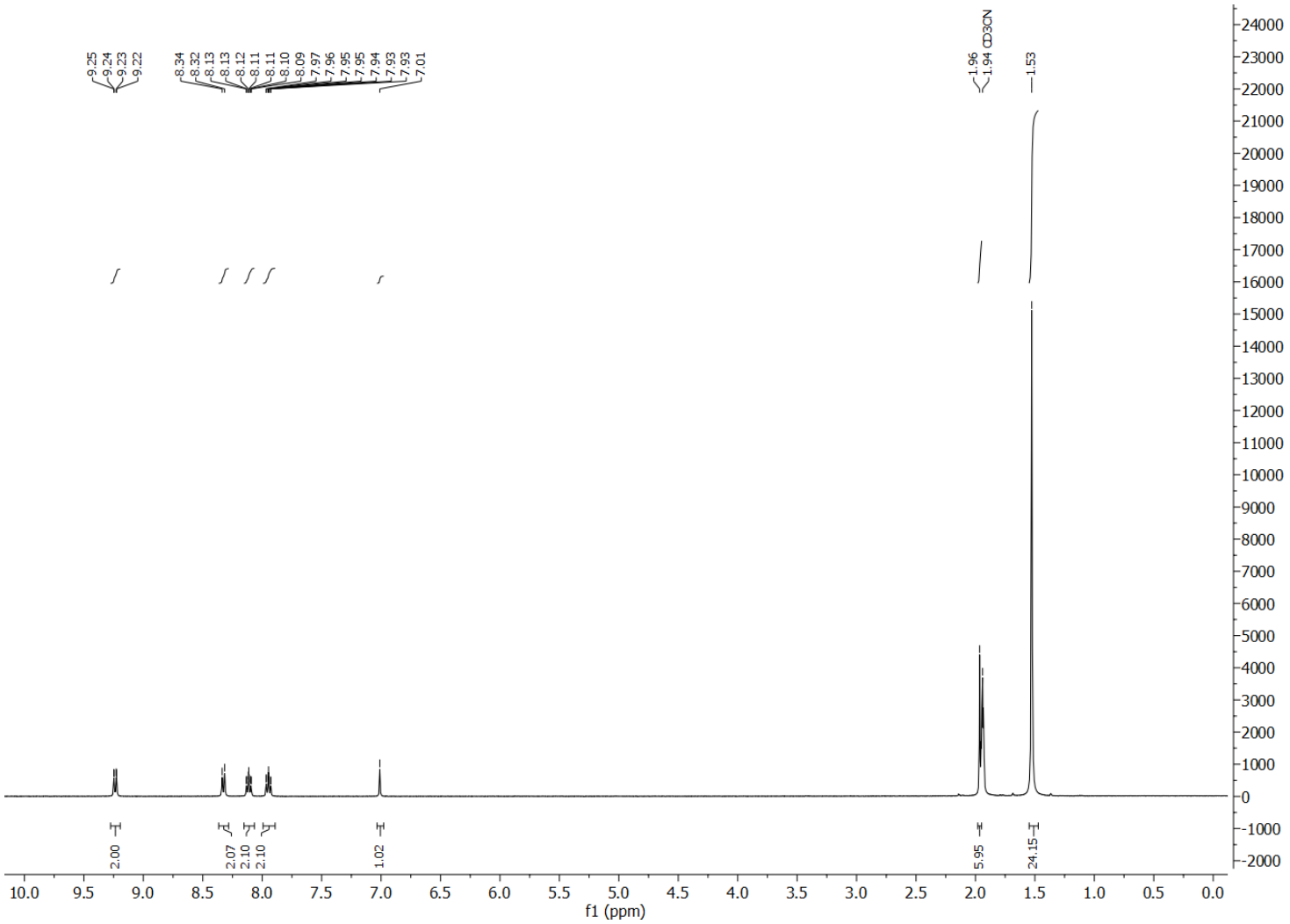


**Fig. S1** $^{1}$H-NMR of [Fe(Mabiq)(MeCN)$_2$]OTf (**1**) in $CD_3CN$.

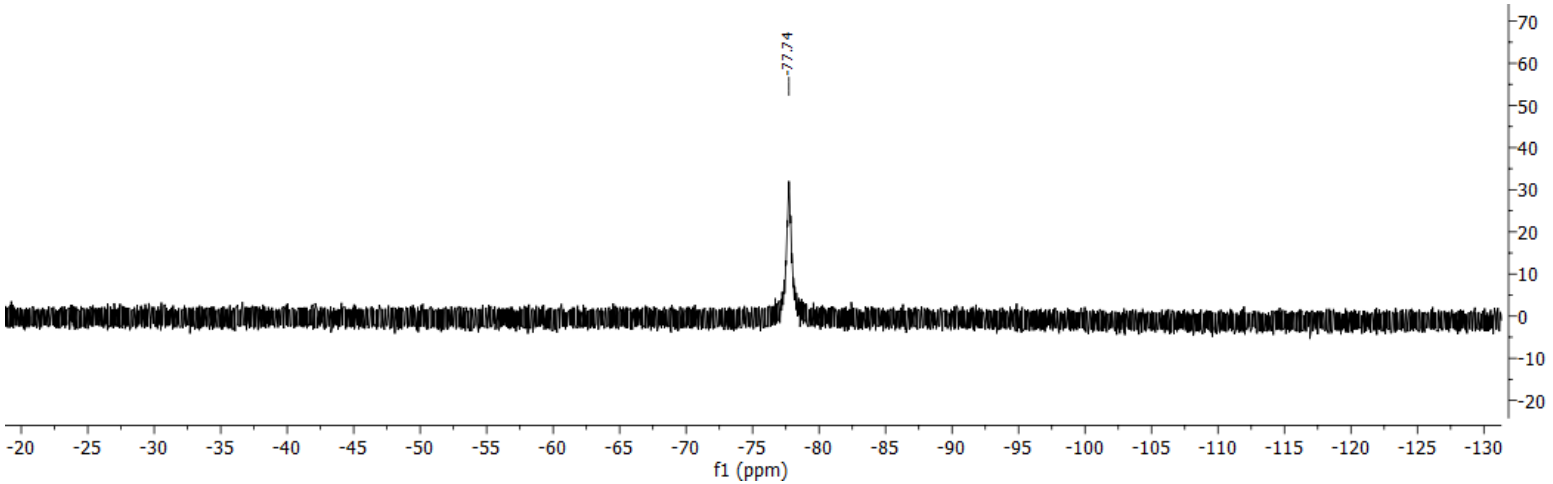


**Fig. S2** $^{19}$F-NMR of **1** in THF-$d_8$.

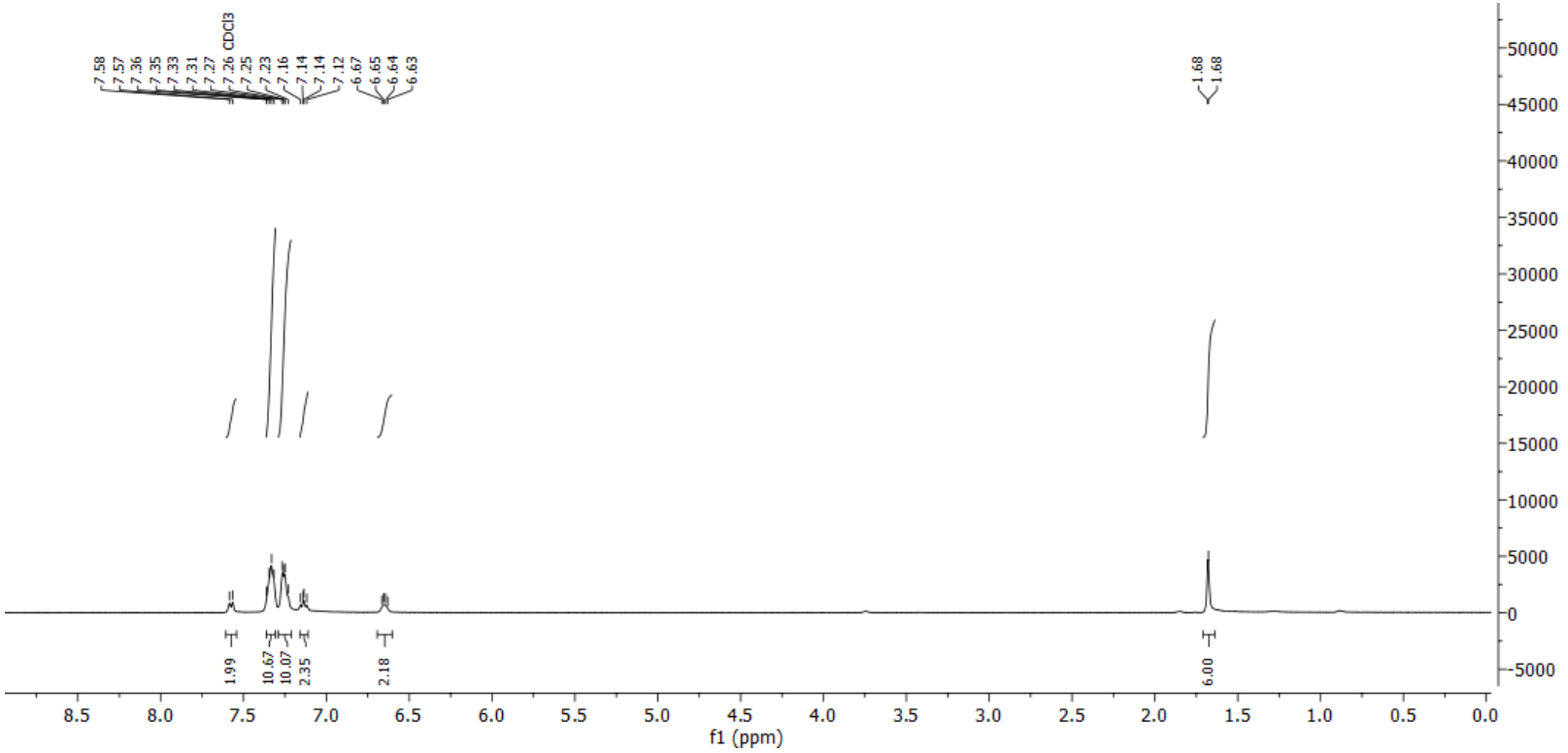


**Fig. S3** $^{1}$H-NMR of [Cu(Xantphos)]OTf (**3**) in $CDCl_3$.

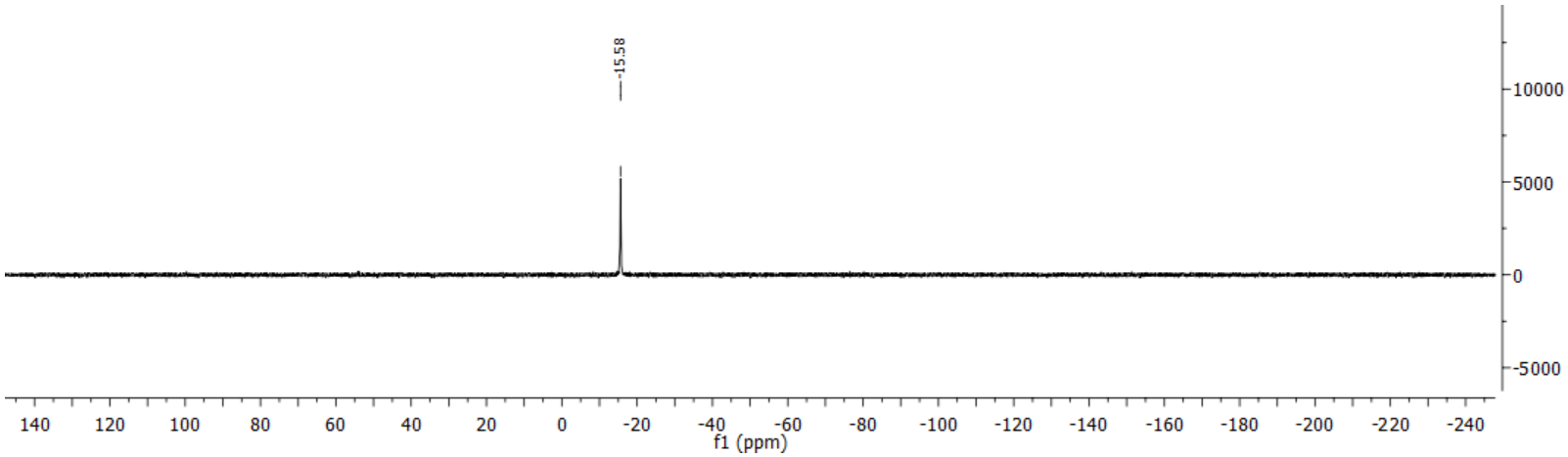


**Fig. S4** $^{31}$P-NMR of **3** in $CDCl_3$.

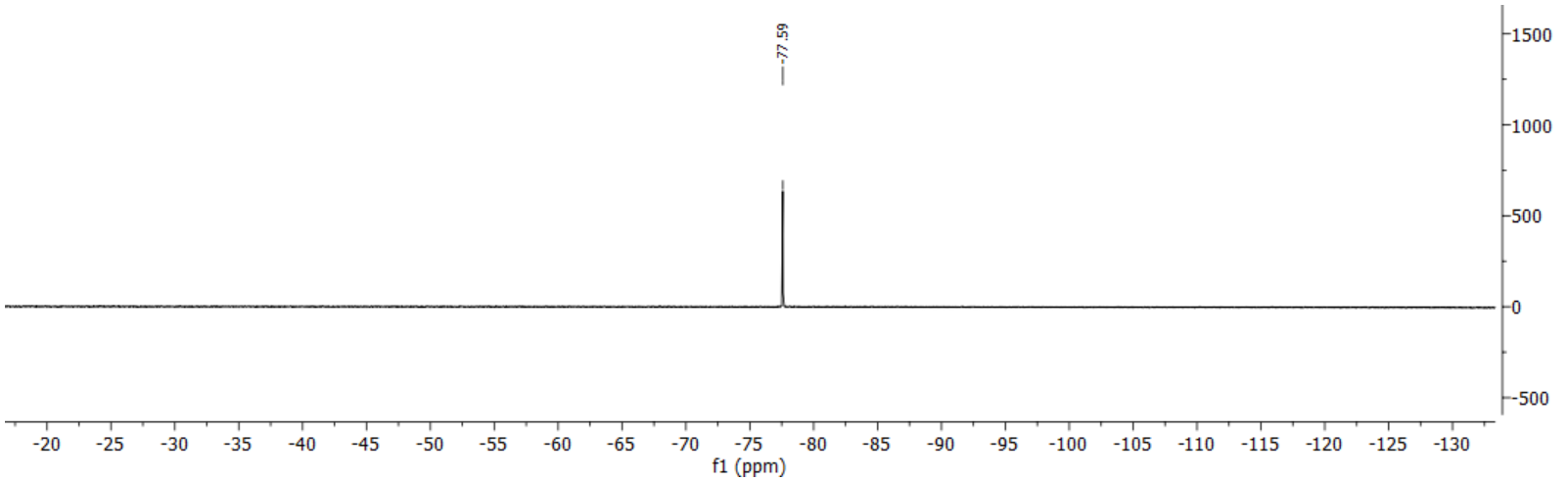


**Fig. S5** $^{19}$F-NMR of **3** in $CD_3CN$.

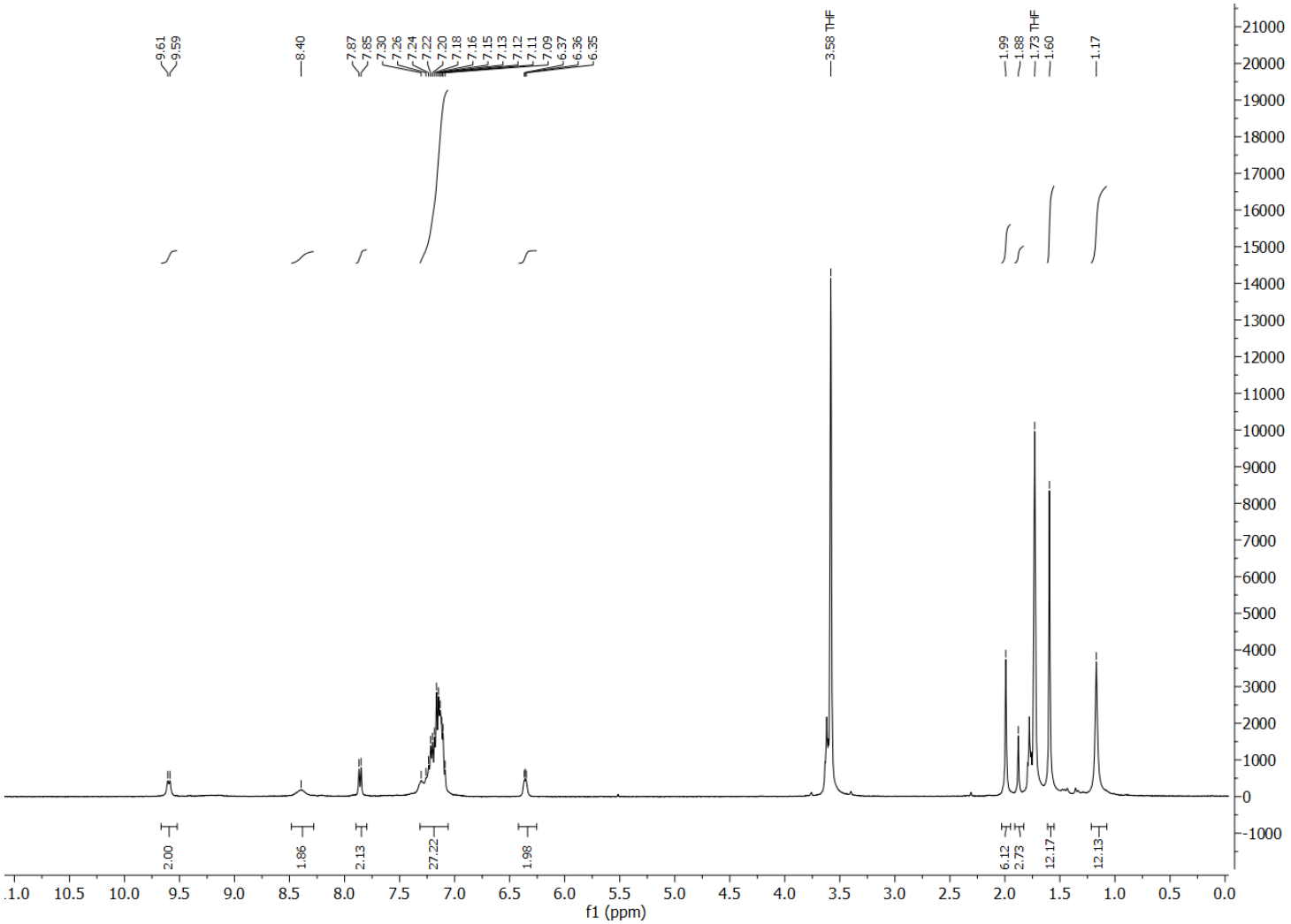


**Fig. S6** $^{1}$H-NMR of [Cu(Xantphos)Fe(Mabiq)(MeCN)(OTf)]OTf (**2**) in THF-$d_8$.

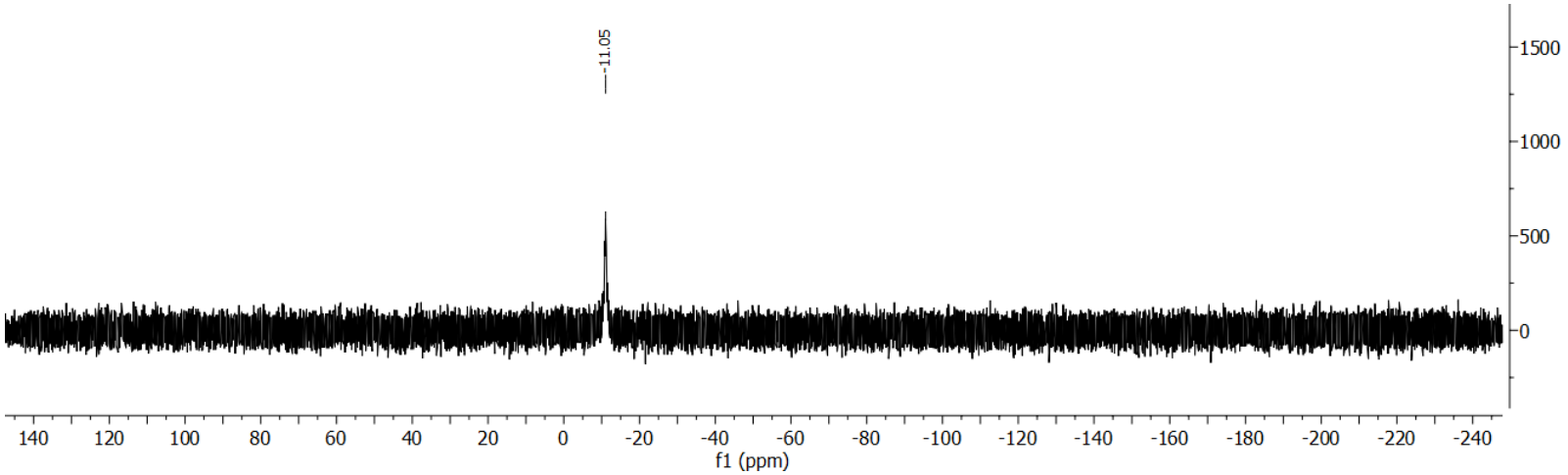


**Fig. S7** $^{31}$P-NMR of **2** in THF-$d_8$.

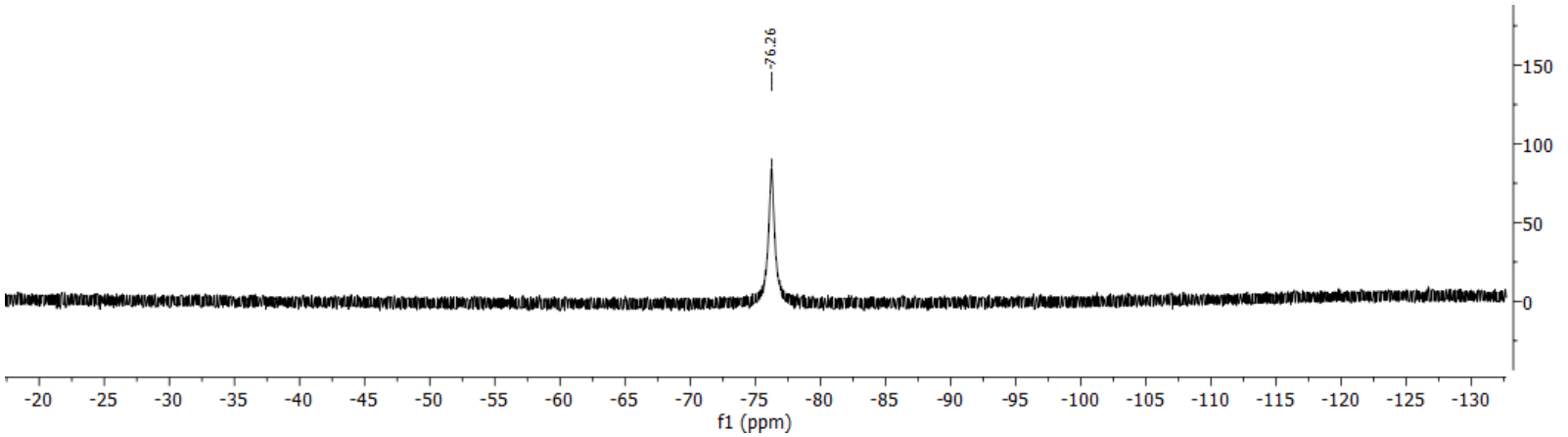


**Fig. S8** $^{19}$F-NMR of **2** in THF-$d_8$.

**Comparison of $^{1}$H-NMR of 1, 2 and 3 in the aromatic region**

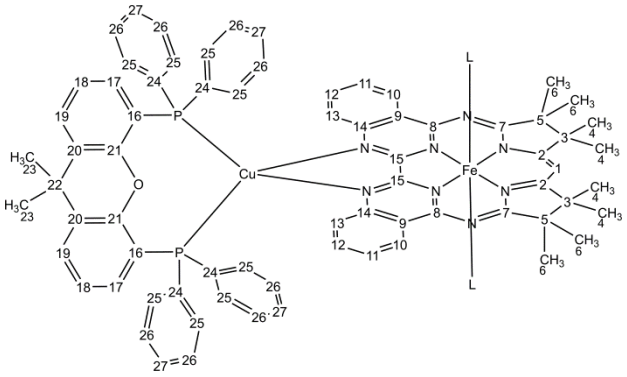

**Chart 1** Numbering scheme of **2** used for NMR figures. The same numbering scheme was used for the monometallic complexes for clarity.

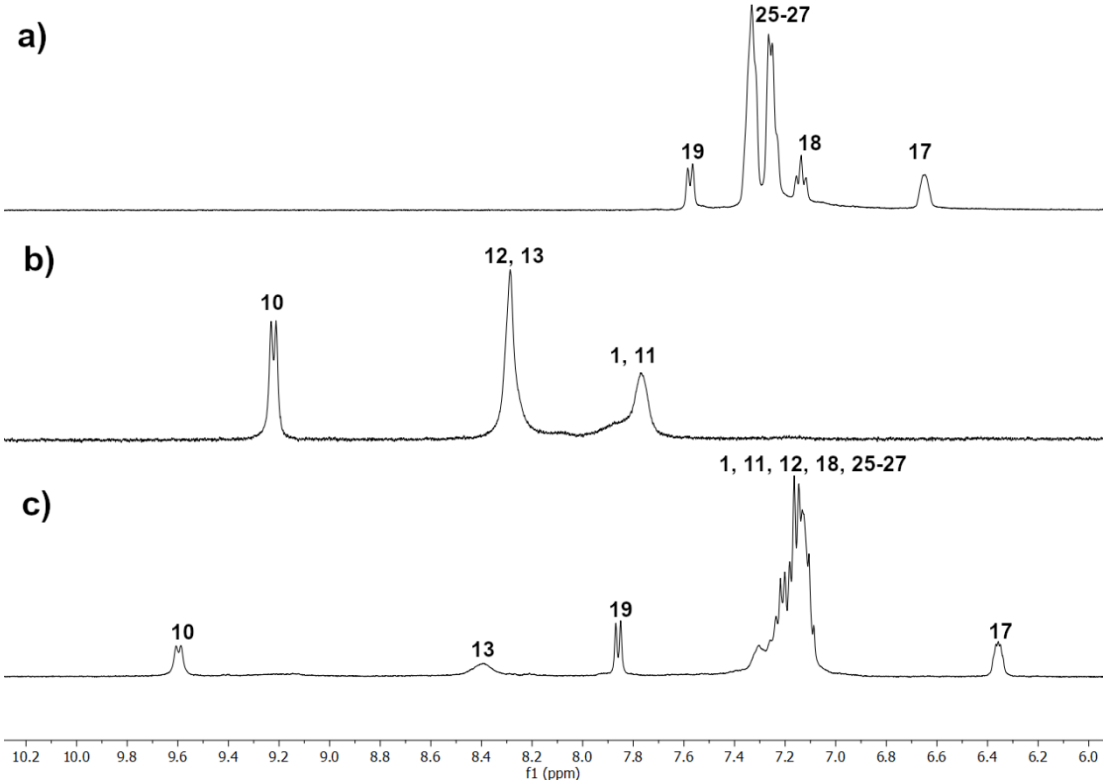


**Fig. S9** Aromatic region of $^{1}$H-NMR spectra of **3** in $CDCl_3$ (**a**), **1** (**b**) and **2** (**c**) in THF-$d_8$. The protons are numbered according to the numbering scheme shown in Chart 1.

**Molecular structure of 2**

For all catalysis experiments **2** was recrystallized from THF/Pentane. Both NMR and elemental analysis indicate one MeCN coordinated to the Fe center (i.e. [Cu(Xantphos)Fe(Mabiq)(MeCN)(OTf)](OTf)). Single crystals suitable for XRD were obtained from DCM/$Et_2O$; the corresponding structure shows both triflate anions coordinated to the Fe center (i.e. [Cu(Xantphos)Fe(Mabiq)$(OTf)_2$]).

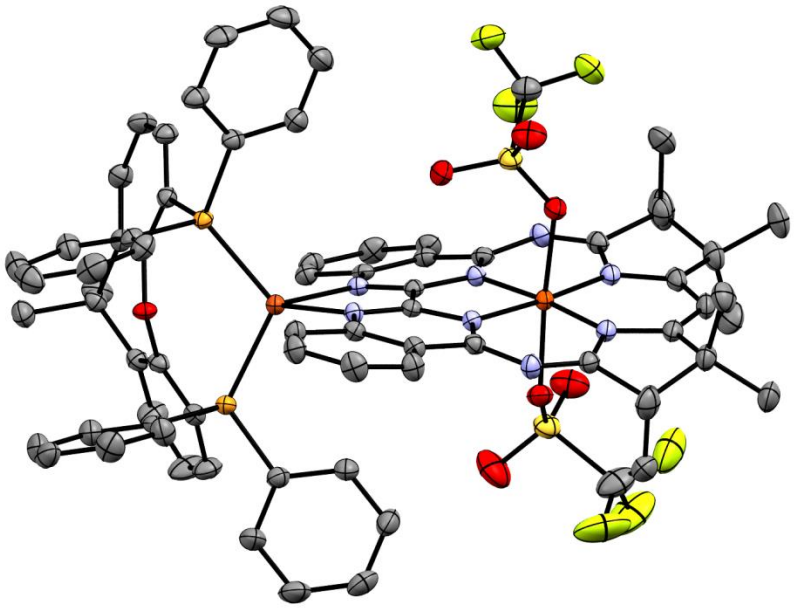

**Fig. S10** ORTEP style representation of the asymmetric unit of **2** in the solid state. Ellipsoids are shown at 50% probability level and hydrogen atoms are omitted for clarity.

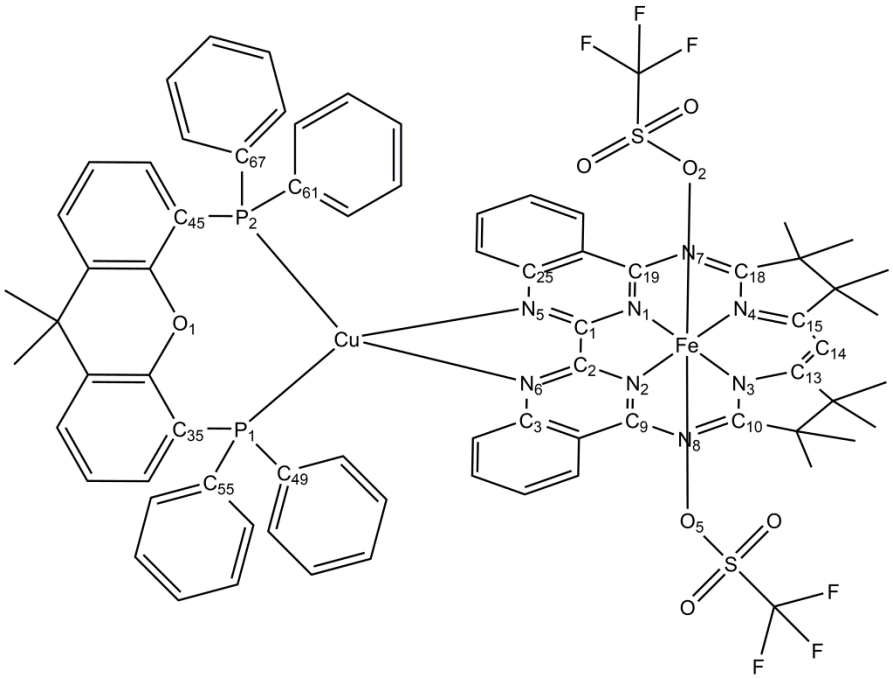


**Chart 2** Atomic numbering scheme for **2**.

**Table S1** Crystallographic parameters for **2**.

| | |
|---|---|
| Empirical formula | $C_{74}H_{65}CuF_6FeN_8O_7P_2S_2$ |
| Formula weight | 1537.80 |
| Crystal system | Triclinic |
| Space group | P −1 |
| a (Å) | 11.046(2) |
| b (Å) | 18.140(3) |
| c (Å) | 10.185(4) |
| α (°) | 81.621(6) |
| β (°) | 86.362(7) |
| γ (°) | 82.139(7) |
| Volume (Å³) | 3959.9(13) |
| Z | 2 |
| ρcalc (g/cm³) | 1.290 |
| μ ($mm^{-1}$) | 0.613 |
| F (000) | 1584 |
| Reflns. Collected | 158292 |
| Indep. reflns/Rint | 14430 |
| Data/restraints/param | 14430/0/920 |
| GOF on F² | 1.062 |
| Final R1 indexes [$I \geq 2\sigma(I)$] | 0.0357 |
| Final wR2 indexes (all data) | 0.0968 |
| Δρmin/max ($eÅ^{-3}$) | −0.500 and 0.412 |
| CCDC number | 2284733 |

**Table S2** Select bond lengths for **2** following the numbering scheme indicated in Chart **2**.

| | |
|---|---|
| Cu1-P1 | 2.2924(8) |
| Cu1-P2 | 2.2711(6) |
| Cu1-N5 | 2.135(2) |
| Cu1-N6 | 2.110(2) |
| | |
| Fe1-O2 | 2.037(2) |
| Fe1-O5 | 2.054(2) |
| Fe1-N1 | 1.925(2) |
| Fe1-N2 | 1.925(2) |
| Fe1-N3 | 1.898(2) |
| Fe1-N4 | 1.905(2) |
| | |
| P1-C35 | 1.830(2) |
| P1-C49 | 1.828(2) |
| P1-C55 | 1.832(2) |
| P2-C45 | 1.831(2) |
| P2-C61 | 1.823(2) |
| P2-C67 | 1.832(2) |
| | |
| N1-C1 | 1.362(2) |
| N1-C19 | 1.346(3) |
| N2-C2 | 1.362(2) |
| N2-C9 | 1.346(3) |
| N3-C10 | 1.368(3) |
| N3-C13 | 1.355(3) |
| N4-C15 | 1.352(3) |
| N4-C18 | 1.368(3) |
| N5-C1 | 1.312(3) |
| N5-C25 | 1.382(2) |
| N6-C2 | 1.305(2) |
| N6-C3 | 1.386(3) |
| C1-C2 | 1.471(3) |
| C13-C14 | 1.388(3) |
| C14-C15 | 1.384(3) |

**Table S3** Select bond angles of **2** following the numbering scheme indicated in Chart **2**.

| | |
|---|---|
| P1-Cu1-P2 | 113.48(2) |
| P1-Cu1-N5 | 114.16(5) |
| P1-Cu1-N6 | 110.79(5) |
| P2-Cu1-N5 | 113.75(5) |
| P2-Cu1-N6 | 121.14(5) |
| N5-Cu1-N6 | 79.30(6) |
| | |
| O2-Fe1-O5 | 174.08(6) |
| O2-Fe1-N1 | 96.20(7) |
| O2-Fe1-N2 | 92.08(7) |
| O2-Fe1-N3 | 87.46(7) |
| O2-Fe1-N4 | 86.66(7) |
| | |
| N1-Fe1-N2 | 84.29(7) |
| N1-Fe1-N4 | 90.84(7) |
| N2-Fe1-N3 | 91.05(7) |
| N3-Fe1-N4 | 93.92(7) |
| | |
| N5-C1-C2 | 117.9(2) |
| C2-N2-C9 | 117.9(2) |
| C1-N1-C19 | 118.4(2) |
| N6-C2-C1 | 118.2(2) |
| C13-C14-C15 | 125.9(2) |

**Absorption spectra of 1 and 2**

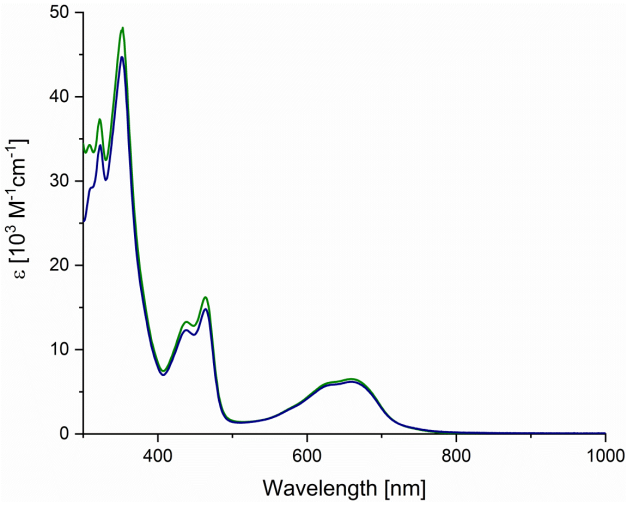


**Fig. S11** UV-Vis absorption spectra of **1** (blue) and **2** (green) in MeCN.

**IR spectra of 1 and 2**

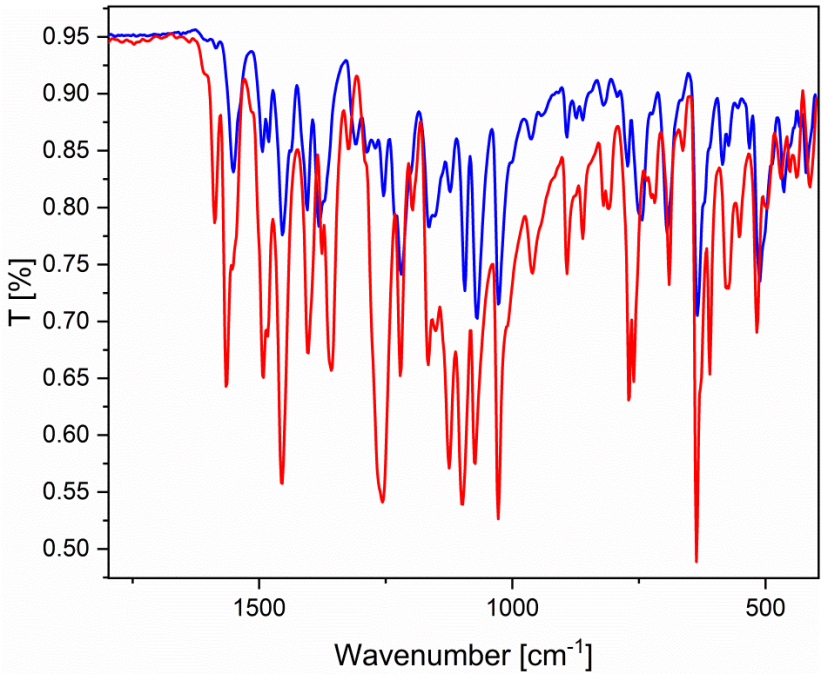


**Fig. S12** IR spectra of **1** (red) and **2** (blue) in the solid state.

To assess whether the bimetallic complex dissociates in solution the IR spectrum of **2** in MeCN was compared with a mathematically combined spectrum of **1** and **3** in MeCN. The shifts in the fingerprint region suggest the complex remains stable in solution.

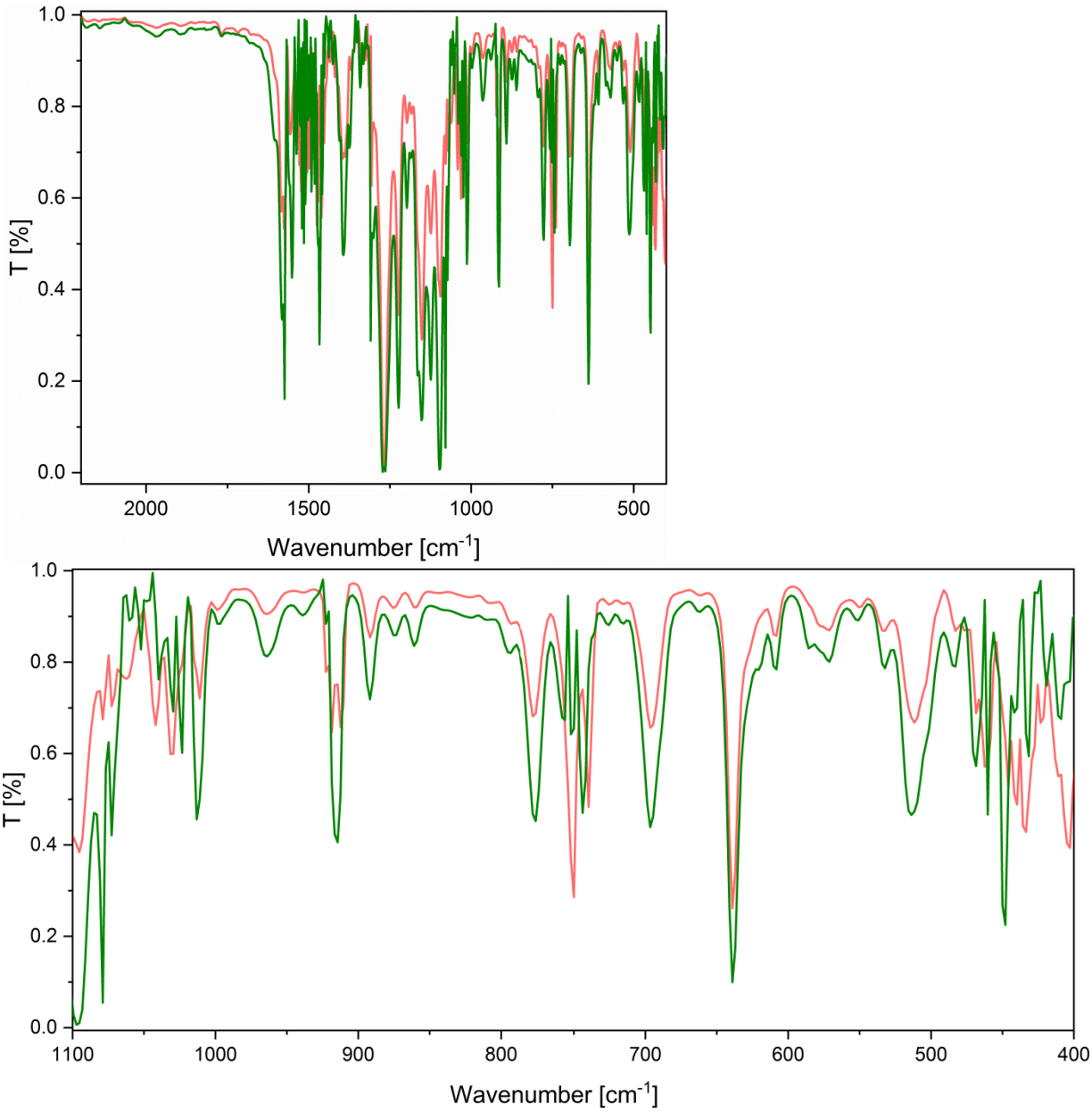


**Fig. S13** Top: IR spectrum of a 6 mM solution of **2** in MeCN (green) in comparison to a mathematical combination of solution IR spectra of **1** and **3** (red) Bottom: Zoom-in of the fingerprint region of the upper IR spectra.

**CV data for 1 and 2**

**Table S4** Comparison of redox potentials of **1** and **2** in MeCN.

| Complex | $Fe^{III/II}$ | $Mabiq/Mabiq^{\bullet-}$ | $Mabiq^{\bullet-}/Mabiq^{2-}$ | $[Fe(Mabiq)]^{-/2-}$ |
|---|---|---|---|---|
| **1** | 0.60 $V_{Fc}$ | −1.31 $V_{Fc}$ | −1.65 $V_{Fc}$ | −2.35 $V_{Fc}$ |
| **2** | 0.62 $V_{Fc}$ | −1.17 $V_{Fc}$ | −1.50 $V_{Fc}$ | −1.95 $V_{Fc}$ |

**[PhOH] dependence of 2**

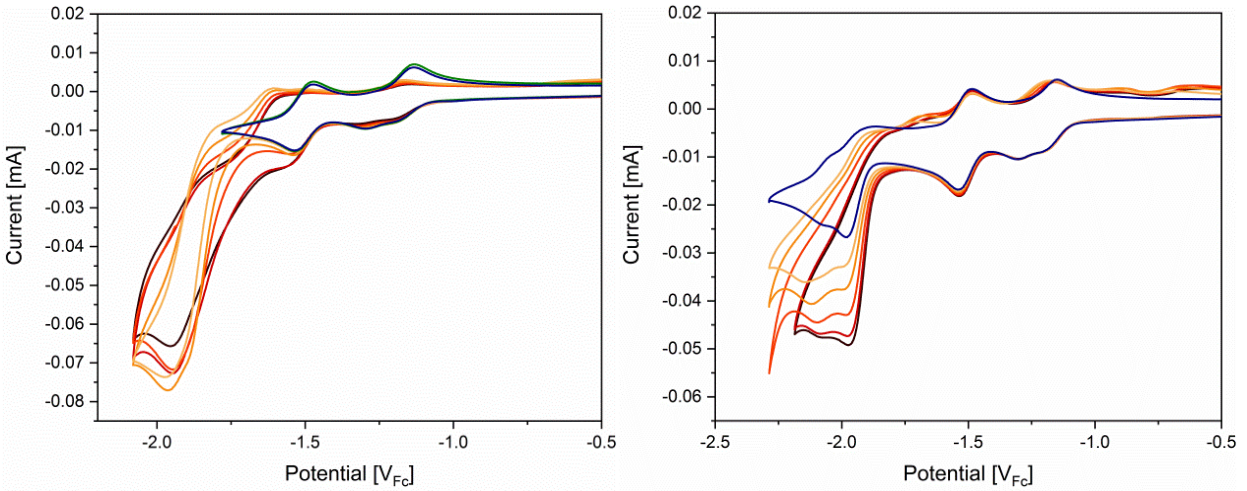


**Fig. S14** CV of a 0.5 mM solution of **2** (blue) in MeCN (0.1 M $[(n\text{-Bu})_4N]PF_6$) with varying amounts of PhOH (Yellow to black: 10, 25, 50, 75 and 85 equiv.) in the presence (left, green: after purging with $CO_2$) and absence (right) of $CO_2$.

**Headspace analysis after photocatalysis experiments**

Various control experiments were conducted to confirm $CO_2$ as the product source. In the absence of $CO_2$ (Ar atmosphere) no significant amounts of CO were detected (Table S5) such that the CO produced under standard conditions does not originate from organic degradation

products. Experiments using isotopically labelled $^{13}CO_2$ further confirmed $CO_2$ as the product source (Fig. S17). Analysis of the liquid phase of the reaction mixtures by $^{1}H$- and $^{13}C$-NMR did not reveal any other reaction products.

**Table S5** Analysis of photocatalytic $CO_2$ reduction by **1** and **2**.

| entry | complex | deviation from standard conditions | $n_{CO}$ [μmol] | $TON_{CO}$ | $TOF_{CO}$ [$s^{-1}$] |
|---|---|---|---|---|---|
| 1 | **1** | - | 2.65 ± 0.24 | 663 ± 61 | 0.18 ± 0.02 |
| 2 | **2** | - | 3.77 ± 0.39 | 942 ± 98 | 0.26 ± 0.03 |
| 3 | **1** | No light | 0.0019 ± 0.001 | 0.4 ± 0.3 | $(13 \pm 9)\times10^{-5}$ |
| 4 | **2** | No light | 0.0016 ± 0.001 | 0.4 ± 0.3 | $(11 \pm 7)\times10^{-5}$ |
| 5 | **1** | No $CO_2$ | 0.005 ± 0.006 | 1 ± 1 | $(3.6 \pm 3.9)\times10^{-4}$ |
| 6 | **2** | No $CO_2$ | 0.004 ± 0.003 | 1 ± 0.6 | $(2.7 \pm 2)\times10^{-4}$ |
| 7 | **1** | No BIH | 0.005 ± 0.002 | 1.3 ± 0.5 | $(4 \pm 2)\times10^{-4}$ |
| 8 | **2** | No BIH | 0.006 ± 0.001 | 1.5 ± 0.3 | $(43 \pm 9)\times10^{-5}$ |
| 9 | **1** | 0.05 mL Hg | 1.9 ± 0.2 | 469 ± 59 | 0.13 ± 0.02 |
| 10 | **2** | 0.05 mL Hg | 3.1 ± 0.2 | 784 ± 55 | 0.22 ± 0.015 |
| 11 | **No** | No catalyst | 0.07 ± 0.03 | - | - |
| 12 | **3** | - | 0.089 ± 0.007 | -* | -* |
| 13 | **4** | - | 0.013 ± 0.01 | -* | -* |
| 14 | **1** | No **Ru-PS** | $(50 \pm 5)\times10^{-4}$ | 1.3 ± 0.12 | $(35 \pm 3)\times10^{-5}$ |
| 15 | **2** | No **Ru-PS** | 0.37 ± 0.1 | 92 ± 30 | 0.025 ± 0.008 |
| 16 | **2** | No **Ru-PS**, 0.05 mL Hg | 0.94 ± 0.33 | 236 ± 82 | 0.065 ± 0.023 |

Standard conditions: 2 μM complex (**1**, **2** or **3**), 170 μM PhOH, 200 μM **Ru-PS**, 100 mM BIH in a total volume of 2 mL, purged with $CO_2$ for 2 min, irradiation at 455 nm for 1 h at 20 °C.

* Due to the similar amount of CO produced, it is likely that **Ru-PS** and not **3** or **4** acts as the catalyst in these experiments, therefore no TON and TOF are given for **3** and **4**.

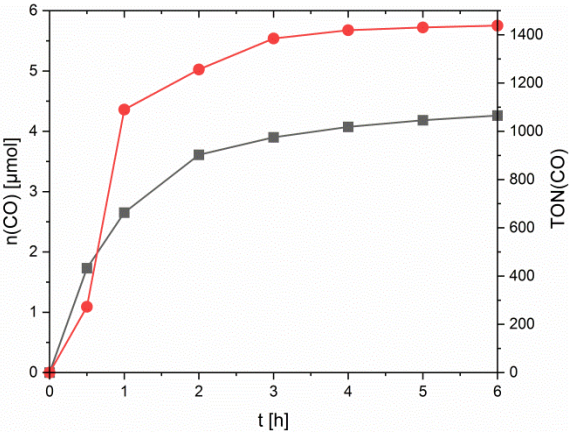


**Fig. S15** CO evolution over time by **1** (black) and **2** (red) under standard conditions.

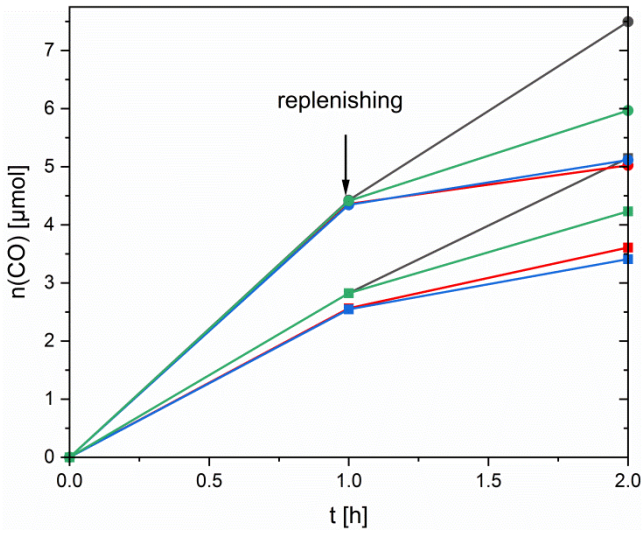


**Fig. S16** CO production by **1** (squares) and **2** (dots) with replenishing of $CO_2$ (red), BIH/**Ru-PS**/$CO_2$ (blue), catalyst/$CO_2$ (green) and catalyst/BIH/**Ru-PS**/$CO_2$ (black) after 1 h. Standard conditions: 2 µM catalyst, 170 µM PhOH, 200 µM **Ru-PS**, 100 mM BIH.

For analysis of the gaseous headspace sample by MS, the headspace sample was taken using a gastight syringe equipped with a valve. The sample was loaded onto the spectrometer by opening the valve of the syringe after which it was slowly drawn into the machine due to the vacuum applied by an internal pump. This is reflected in the shape of the signal. The retention time depended on the time point the valve was opened. The spectrometer was set to monitor a mass of 29 which corresponds to the $^{13}CO$.

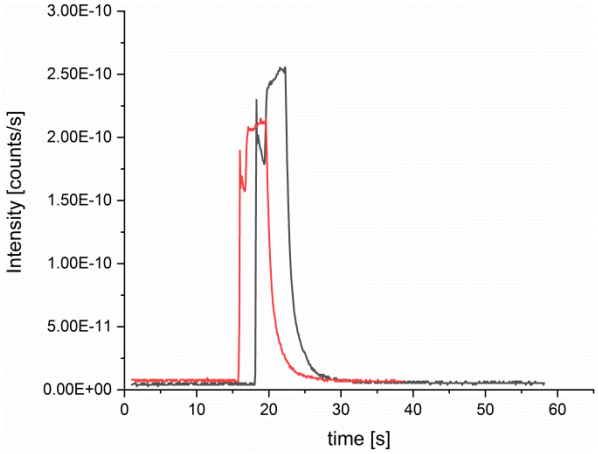


**Fig. S17** MS analysis of the headspace after photocatalytic $CO_2$ reduction by **1** (red) and **2** (black) using $^{13}CO_2$ monitoring a mass of 29.

The precipitation of $BI^+$ in our experiments—the degradation product of BIH after donating two electrons and one proton—(confirmed by $^1$H-NMR, see Fig. S18) prevented the use of dynamic light scattering (DLS) to assess nanoparticle formation.

**NMR of precipitate after photocatalysis**

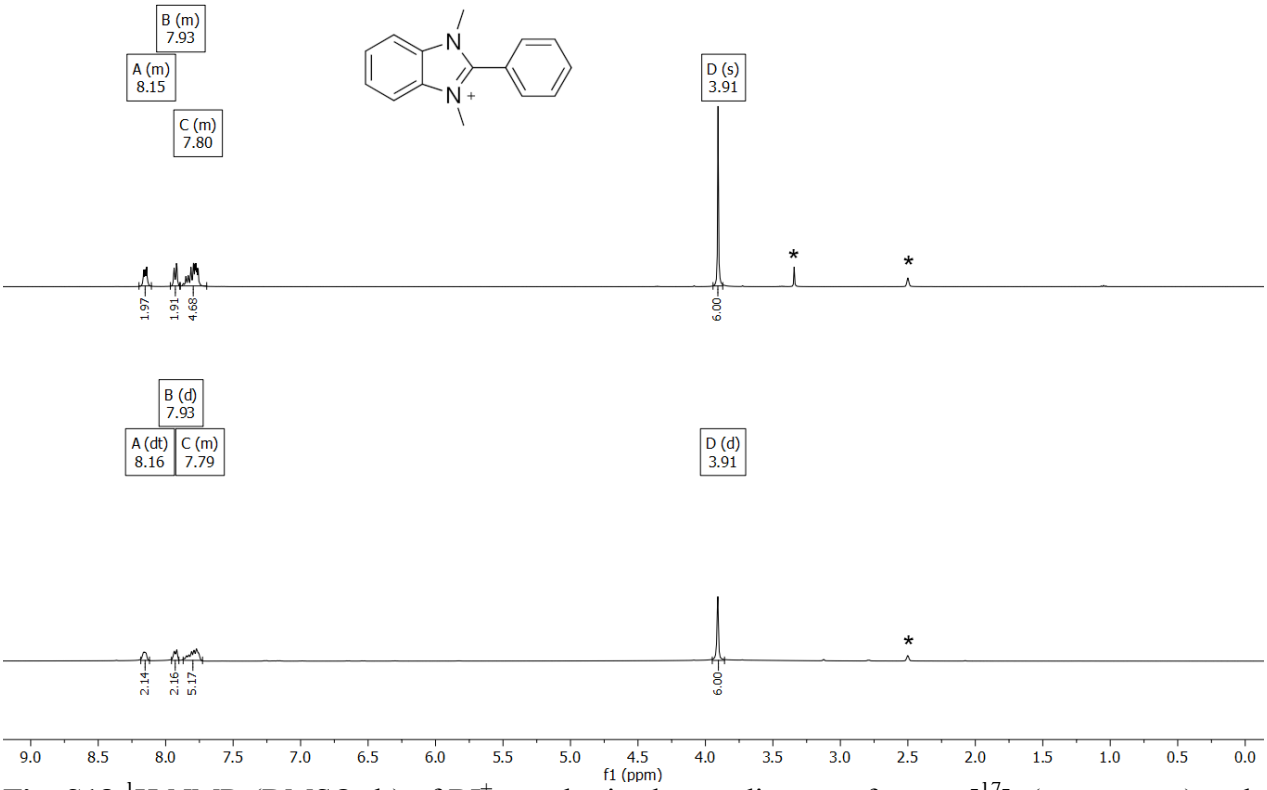


**Fig. S18** $^1$H-NMR (DMSO-$d_6$) of $BI^+$, synthesized according to reference [[17]], (upper trace) and the solid isolated (lower trace) after photocatalytic $CO_2$ reduction by **1** or **2**, respectively, under standard conditions (2 µM catalyst, 200 µM **Ru-PS**, 170 µM PhOH, 100 mM BIH, purged with $CO_2$ for 2 min, irradiated at 455 nm for 1 h at 20 °C). Residual solvent signals (DMSO and $H_2O$ in DMSO) are marked with an asterisk.

**Concentration dependence for photocatalytic $CO_2$ reduction**

**Table S6** Catalyst concentration dependence for photocatalytic $CO_2$ reduction.

| entry | complex | $c_{complex}$ [µM] | $n_{CO}$ [µmol] | $TON_{CO}$ | TOF [$s^{-1}$] |
|---|---|---|---|---|---|
| 1 | **1** | 0.5 | 0.77 ± 0.09 | 765 ± 87 | 0.21 ± 0.02 |
| 2 | **1** | 2 | 2.65 ± 0.24 | 663 ± 61 | 0.18 ± 0.02 |
| 3 | **1** | 50 | 14 ± 2 | 139 ± 17 | 0.039 ± 0.005 |
| 4 | **2** | 0.5 | 0.1 ± 0.004 | 114 ± 4 | 0.03 ± 0.001 |
| 5 | **2** | 2 | 3.77 ± 0.4 | 942 ± 98 | 0.26 ± 0.03 |
| 6 | **2** | 50 | 17 ± 3 | 172 ± 32 | 0.048 ± 0.009 |

Standard conditions: 85 equiv. PhOH, 200 µM **Ru-PS**, 100 mM BIH in a total volume of 2 mL, purged with $CO_2$ for 2 min, irradiated at 455 nm for 1 h at 20 °C.

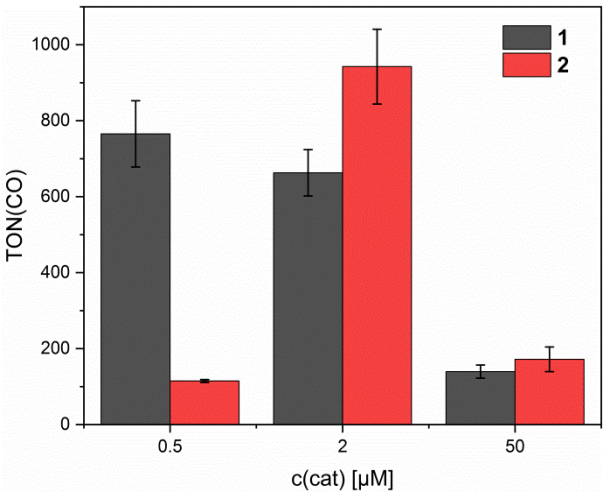


**Fig. S19** Photocatalytic $CO_2$ reduction by **1** (black) and **2** (red) at different catalyst concentrations. Standard conditions: 100 mM BIH, 200 µM **Ru-PS**, 85 equiv. PhOH, $CO_2$, irradiation at 455 nm for 1 h at 20 °C.

**Proton source dependence for photocatalytic $CO_2$ reduction by 1 and 2**

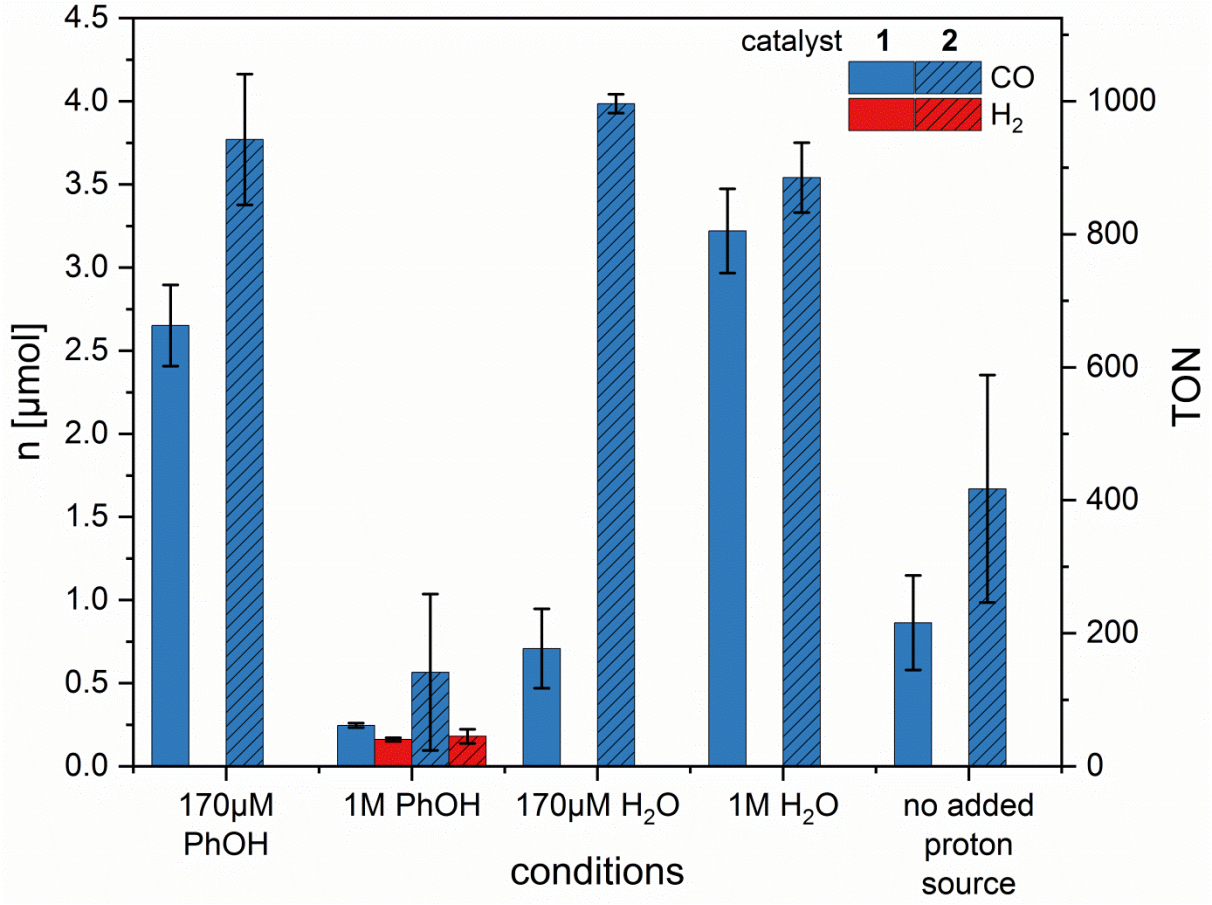


**Fig. S20** Results of analysis for photocatalytic $CO_2$ reduction by **1** (solid columns) and **2** (dashed column) using varying amounts of PhOH or $H_2O$ as proton source. Blue bars depict the amount of CO produced; red bars the amount of $H_2$ produced. Standard conditions: 2 µM catalyst, 200 µM Ru-PS, 100 mM BIH, proton source and $CO_2$. The solutions were irradiated for 1 h at 455 nm at 20 °C.

**Table S7** Proton source dependence on photocatalytic $CO_2$ reduction by **1** and **2**.

| Entry | Complex | Proton source | $n_{CO}$ [μmol] | $TON_{CO}$ | $TOF_{CO}$ [$s^{-1}$] | $n_{H2}$ [μmol] | $TON_{H2}$ | $TOF_{H2}$ [$s^{-1}$] |
|---|---|---|---|---|---|---|---|---|
| 1 | **1** | 170 μM PhOH | 2.65 ± 0.24 | 663 ± 61 | 0.18 ± 0.02 | | | |
| 2 | **1** | 1 M PhOH | 0.25 ± 0.01 | 62 ± 3 | 0.0171 ± 0.0009 | 0.16 ± 0.01 | 40 ± 3 | 0.0112 ± 0.0008 |
| 3 | **1** | 170 μM $H_2O$ | 0.7 ± 0.2 | 177 ± 60 | 0.05 ± 0.02 | | | |
| 4 | **1** | 1 M $H_2O$ | 3.2 ± 0.3 | 805 ± 63 | 0.22 ± 0.02 | | | |
| 5 | **1** | None | 0.86 ± 0.28 | 216 ± 71 | 0.06 ± 0.02 | | | |
| 6 | **2** | 170 μM PhOH | 3.77 ± 0.4 | 942 ± 98 | 0.26 ± 0.03 | | | |
| 7 | **2** | 1 M PhOH | 0.56 ± 0.47 | 141 ± 117 | 0.04 ± 0.03 | 0.18 ± 0.04 | 45 ± 11 | 0.013 ± 0.003 |
| 8 | **2** | 170 μM $H_2O$ | 3.99 ± 0.06 | 996 ± 14 | 0.277 ± 0.004 | | | |
| 9 | **2** | 1 M $H_2O$ | 3.5 ± 0.2 | 885 ± 53 | 0.25 ± 0.01 | | | |
| 10 | **2** | None | 1.7 ± 0.7 | 417 ± 171 | 0.12 ± 0.05 | | | |

Standard conditions: 2 μM catalyst, 200 μM **Ru-PS**, 100 mM BIH in a total volume of 2 mL, purged with $CO_2$ for 2 min, irradiated at 455 nm for 1 h at 20 °C.

**CV of 1 and 2 in the presence of $H_2O$ and $CO_2$**

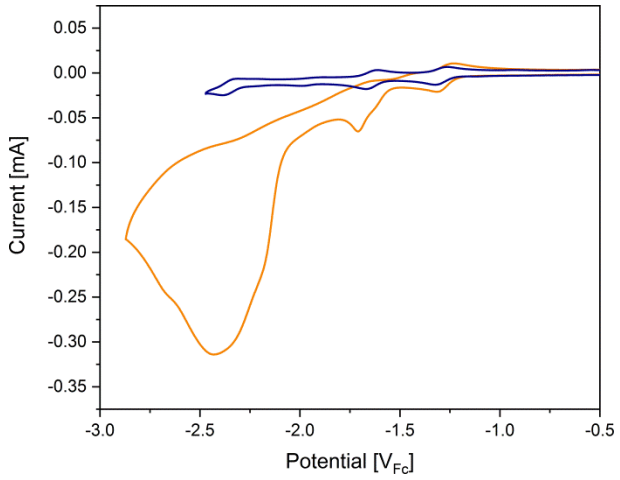


**Fig. S21** CV of **1** (0.5 mM) under Ar atmosphere (blue) and Orange: in the presence of $CO_2$ and 1 M $H_2O$ (0.1 M $[N(n\text{-}Bu)_4]PF_6$ in MeCN, scan rate 100 mV/s).

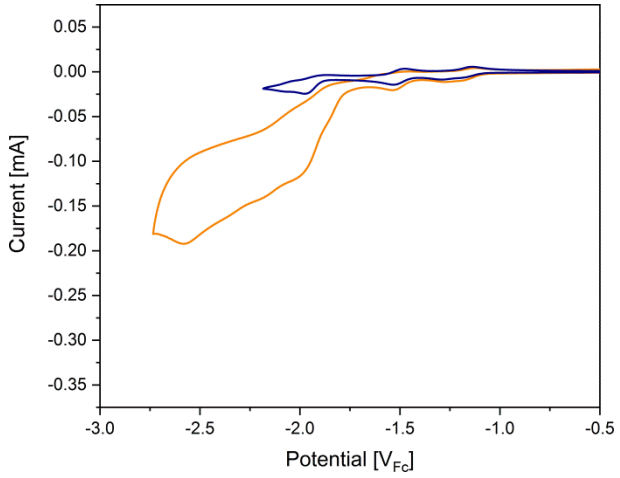


**Fig. S22** CV of **2** (0.5 mM) under Ar atmosphere (blue) and Orange: in the presence of $CO_2$ and 1 M $H_2O$ (0.1 M $[N(n\text{-}Bu)_4]PF_6$ in MeCN, scan rate 100 mV/s).

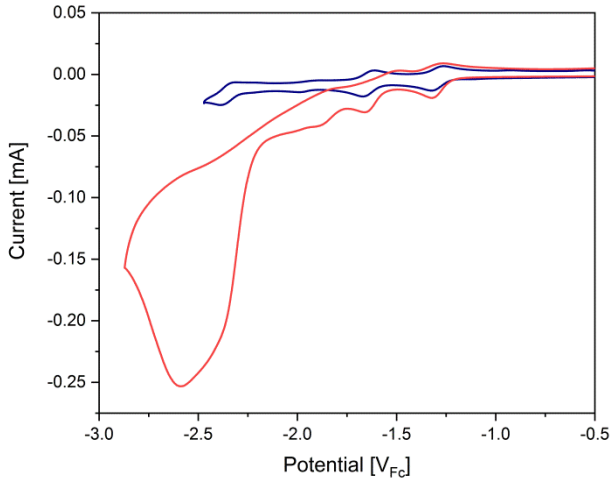


**Fig. S23** CV of **1** (0.5 mM) under Ar atmosphere (blue) and Red: in the presence of $CO_2$ and 100 equiv. $H_2O$ (0.1 M $[N(n\text{-}Bu)_4]PF_6$ in MeCN, scan rate 100 mV/s).

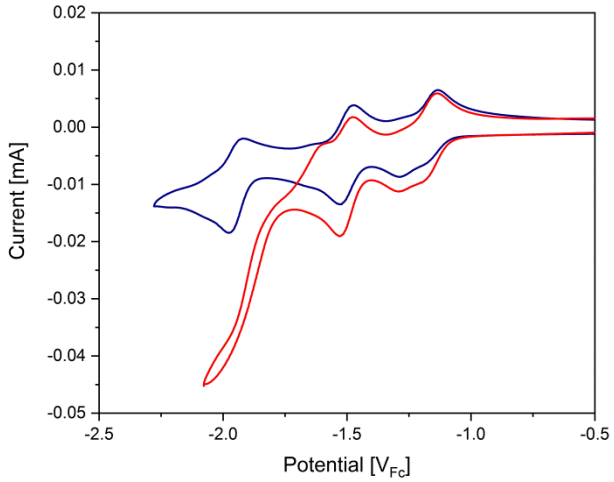


**Fig. S24** CV of **2** (0.5 mM) under Ar atmosphere (blue) and Red: in the presence of $CO_2$ and 100 equiv. $H_2O$ (0.1 M $[N(n\text{-}Bu)_4]PF_6$ in MeCN, scan rate 100 mV/s).

**Quantum Yield Determination experiments for the photoreduction of 1 and 2**

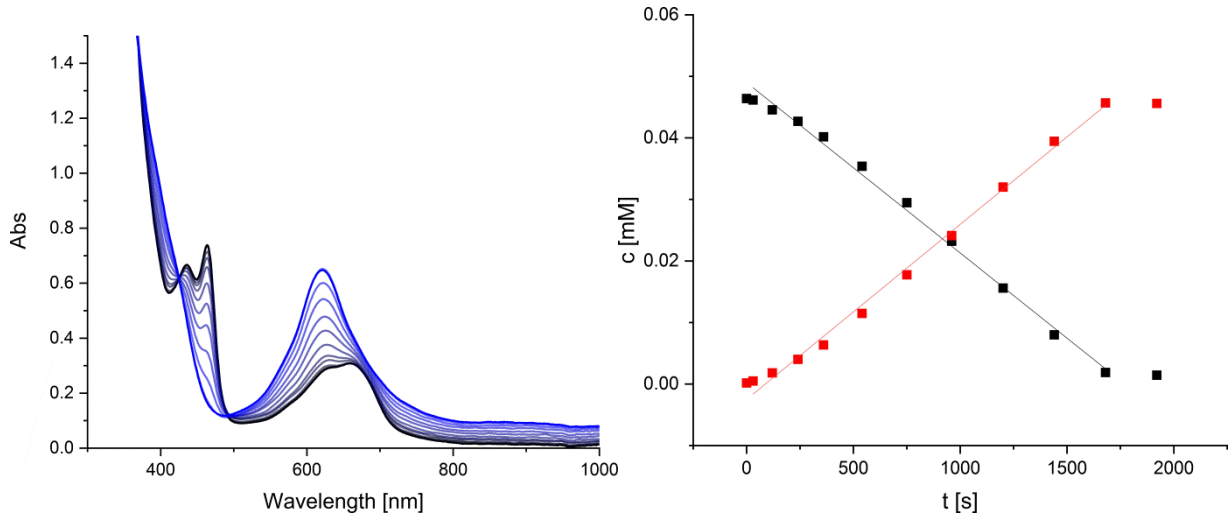


**Fig. S25** Photoreduction of **1** (50 µM) in MeCN using 500 equiv. of BIH as SED. Left: UV-Vis spectral evolution from 0 to 2000 s (initial spectrum shown in black). Right: Concentration vs time plot of [Fe(Mabiq)] formation (red) and the consumption of **1** (black) with linear fit for quantum yield determination (QYD). For the QYD the absorption at 464 nm and 622 nm was monitored.

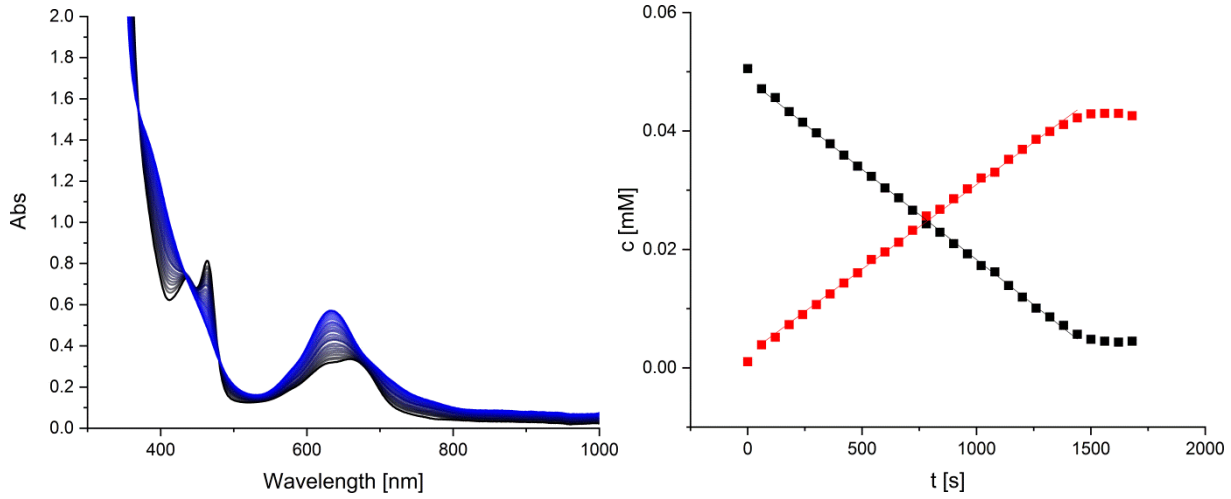


**Fig. S26** Photoreduction of **2** (50 µM) in MeCN using 500 equiv. of BIH as SED. Left: UV-Vis spectral evolution from 0 to 1750 s (initial spectrum shown in black). Right: Concentration vs

time plot of [Cu(Xantphos)Fe(Mabiq)]OTf formation (red) and the consumption of **2** (black) with linear fit for QYD. For the QYD the absorption at 464 nm and 622 nm was monitored.

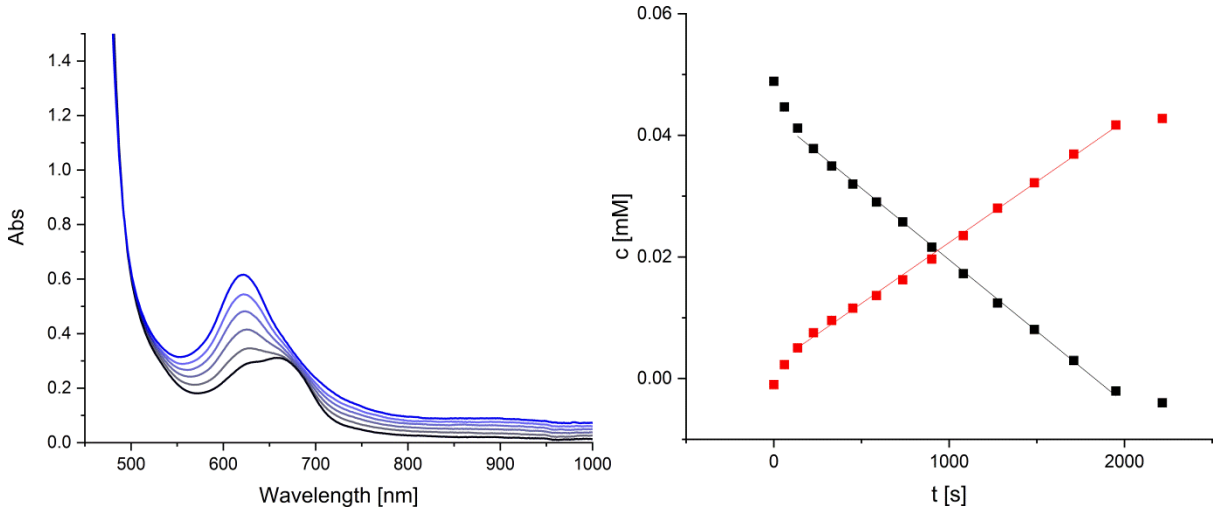


**Fig. S27** Photoreduction of **1** (50 µM) in MeCN using 500 equiv. of BIH as SED and 200 µM **Ru-PS**. Left: UV-Vis spectral evolution from 0 to 2250 s (initial spectrum shown in black). Right: Concentration vs time plot of [Fe(Mabiq)] formation (red) and the consumption of **1** (black) with linear fit for QYD. For the QYD the absorption at 622 nm and 660 nm was monitored.

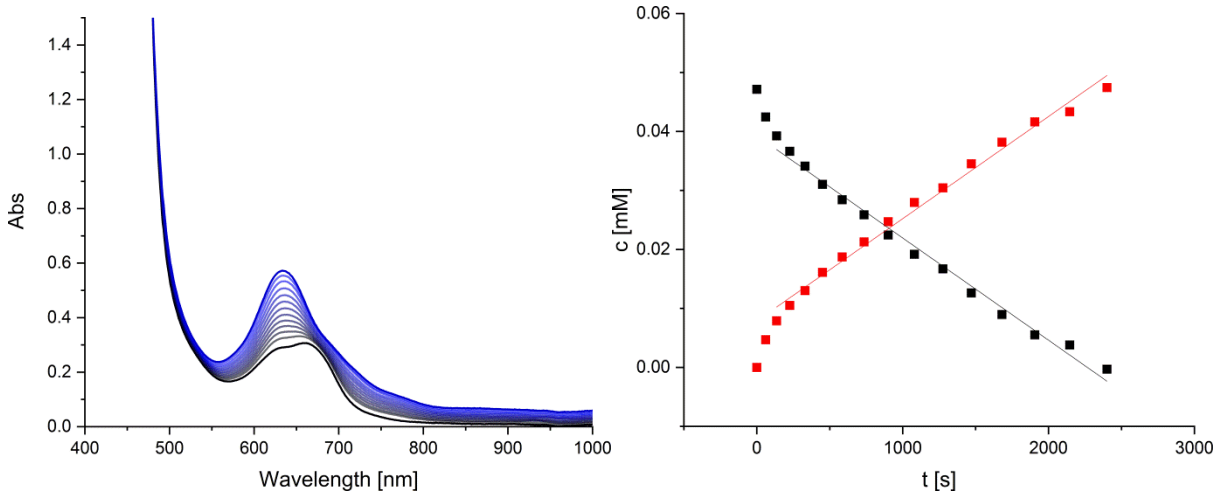


**Fig. S28** Photoreduction of **2** (50 µM) in MeCN using 500 equiv. of BIH as SED and 200 µM **Ru-PS**. Left: UV-Vis spectral evolution from 0 to 2500 s (initial spectrum shown in black). Right: Concentration vs time plot of [Cu(Xantphos)Fe(Mabiq)]OTf formation (red) and the consumption of **2** (black) with linear fit for QYD. For the QYD the absorption at 622 nm and 660 nm was monitored.

**Table S8** Quantum yields for photoreduction of **1** and **2**

| | $P_{ref}$ [mW] | QY | Conversion II→I [%] |
|---|---|---|---|
| **1** + BIH | 302 | $8.02\times10^{-5} \pm 4.3\times10^{-6}$ | 98 ± 2 |
| **2** + BIH | 304 | $5.86\times10^{-5} \pm 8.8\times10^{-6}$ | 77 ± 5 |
| **1** + BIH + **Ru-PS** | 19.75 | $6.5\times10^{-4} \pm 2.3\times10^{-5}$ | 87 ± 3 |
| **2** + BIH + **Ru-PS** | 23.13 | $4.07\times10^{-4} \pm 2.8\times10^{-5}$ | 77 ± 20 |
| **1** + $NEt_3$ [a] | 245 [a] | $1.8\times10^{-4}$ [a] | 100 [a] |

a) Solvent: MeCN:THF, 1:1, taken from Ref. [4]

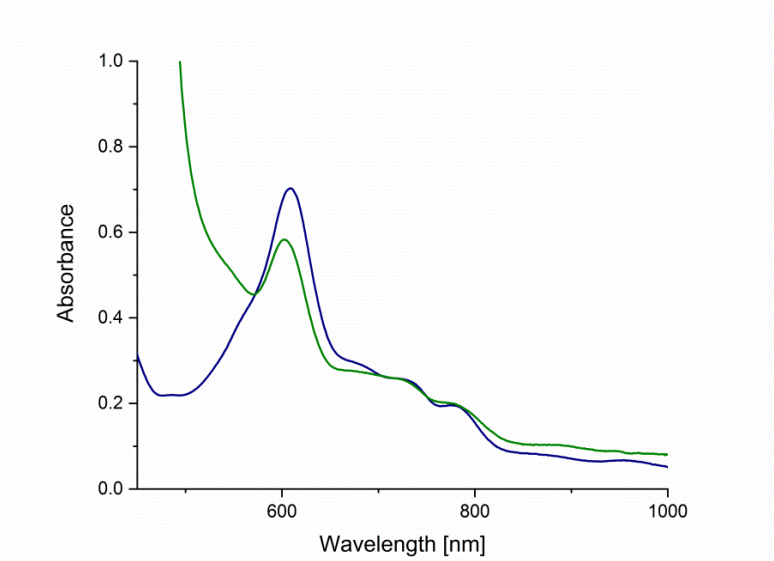


**Fig. S29** Green: Absorption spectrum of the intermediate formed upon irradiation of **1** (50 µM) under photocatalytic conditions (200 µM **Ru-PS**, 25 mM BIH, 170 µM PhOH in MeCN). Blue: Absorption spectrum of the isolated intermediate $\mathbf{I_{PhOH}}$ (50 µM in THF).[21]

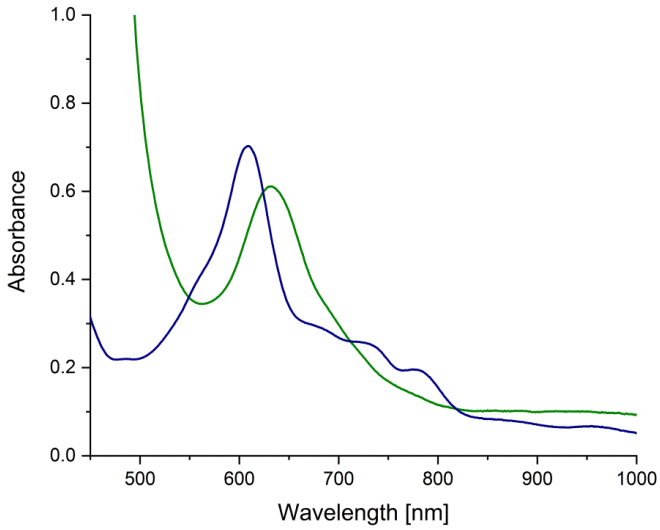


**Fig. S30** Green: Absorption spectrum of the intermediate formed upon irradiation of **2** (50 µM) under photocatalytic conditions (200 µM **Ru-PS**, 25 mM BIH, 170 µM PhOH in MeCN). Blue: Absorption spectrum of $\mathbf{I_{PhOH}}$ (50 µM in THF).[21]

**Molecular structure of 1**

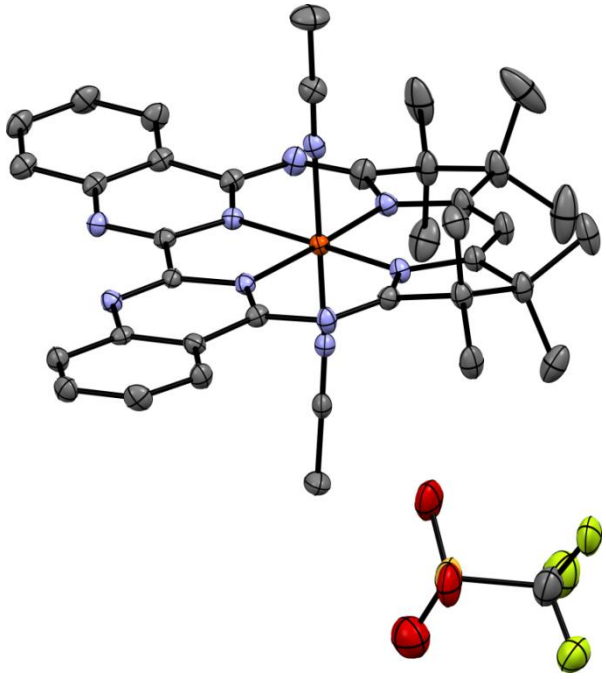

**Fig. S31** ORTEP style representation of the asymmetric unit of **1** in the solid state. Ellipsoids are shown at 50% probability level and hydrogen atoms are omitted for clarity. We observed positional disorder of the triflate counter anion and on the diketiminate backbone; for clarity only one component is shown.

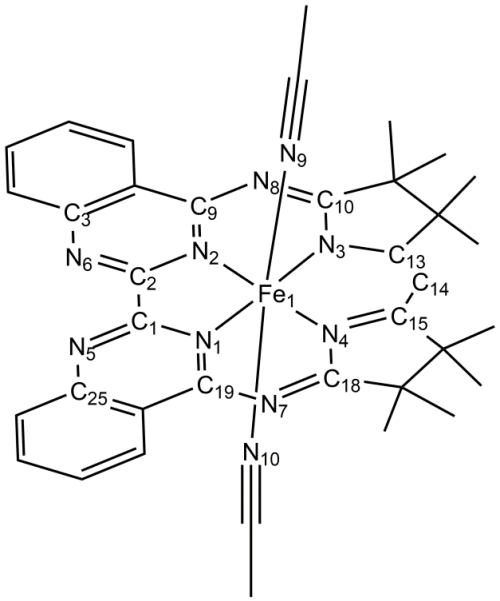


**Chart S3** Atomic numbering in the molecular structure of **1**.

**Table S9** Crystallographic refinement parameters of **1**.

| | |
|---|---|
| Empirical formula | $C_{38}H_{39}F_3FeN_{10}O_3S$ |
| Formula weight | 828.6972 |
| Crystal system | monoclinic |
| Space group | P $2_1$/c |
| a (Å) | 12.8059(19) |
| b (Å) | 16.387(2) |
| c (Å) | 20.403(3) |
| α (°) | 90 |
| β (°) | 105.269(6) |
| γ (°) | 90 |
| Volume (Å³) | 4130.35 |
| Z | 4 |
| ρcalc (g/cm³) | 1.333 |
| μ ($mm^{-1}$) | 0.478 |
| F (000) | 1720 |
| Reflns. Collected | 207033 |
| Indep. reflns/Rint | 7259 |
| Data/restraints/param | 7259/631/712 |
| GOF on F² | 1.123 |
| Final R1 indexes [I ≥ 2σ(I)] | 0.0482 |
| Final wR2 indexes (all data) | 0.1474 |
| Δρmin/max ($eÅ^{-3}$) | −0606 and 1.007 |
| CCDC number | 2284734 |

**Table S10** Select bond lengths for **1**, numbering of atoms as indicated in Chart S3.

| | |
|---|---|
| Fe1-N1 | 1.934(1) |
| Fe1-N2 | 1.939(8) |
| Fe1-N3 | 1.924(0) |
| Fe1-N4 | 1.921(2) |
| Fe1-N9 | 1.944(4) |
| Fe1-N10 | 1.946(5) |
| | |
| C1-C2 | 1.485(0) |
| C1-N1 | 1.375(9) |
| C1-N5 | 1.302(9) |
| C2-N2 | 1.375(7) |
| C2-N6 | 1.307(5) |
| C3-N6 | 1.367(9) |
| N1-C19 | 1.337(8) |
| N2-C9 | 1.335(3) |
| N3-C10 | 1.358(6) |
| N3-C13 | 1.350(3) |
| N4-C15 | 1.358(0) |
| N4-C18 | 1.367(9) |
| N5-C25 | 1.370(9) |
| N7-C18 | 1.299(7) |
| N7-C19 | 1.376(6) |
| N8-C9 | 1.360(4) |
| C13-C14 | 1.392(1) |
| C14-C15 | 1.387(4) |

**Table S11** Select bond angles (°) for **1**, numbering of atoms as indicated in Chart S3.

| | |
|---|---|
| N1-Fe1-N2 | 84.05 |
| N1-Fe1-N3 | 175.03 |
| N1-Fe1-N4 | 91.42 |
| N2-Fe1-N3 | 91.04 |
| N2-Fe1-N4 | 175.12 |
| N3-Fe1-N4 | 93.50 |
| N9-Fe1-N10 | 177.71 |
| | |
| C2-C1-N1 | 113.82 |
| C2-C1-N5 | 118.94 |
| N1-C1-N5 | 127.22 |
| C1-C2-N2 | 113.64 |
| C1-C2-N6 | 119.39 |
| N2-C2-N6 | 126.94 |
| | |
| Fe1-N1-C1 | 114.22 |
| Fe1-N2-C2 | 114.17 |
| Fe1-N3-C13 | 126.51 |
| Fe1-N4-C15 | 126.17 |
| N3-C13-C14 | 123.77 |
| C13-C14-C15 | 125.96 |
| | |
| Fe1-N9-C34 | 177.86 |
| Fe1-N10-C36 | 172.54 |

## References


1. B. D. McCarthy, D. J. Martin, E. S. Rountree, A. C. Ullman and J. L. Dempsey, *Inorg. Chem.*, 2014, **53**, 8350-8361.
2. M. D. Sampson and C. P. Kubiak, *J. Am. Chem. Soc.*, 2016, **138**, 1386-1393.
3. O. Z. Esezobor, W. Zeng, L. Niederegger, M. Grübel and C. R. Hess, *J. Am. Chem. Soc.*, 2022, **144**, 2994-3004.
4. R. Lauenstein, S. L. Mader, H. Derondeau, O. Z. Esezobor, M. Block, A. J. Römer, C. Jandl, E. Riedle, V. R. I. Kaila, J. Hauer, E. Thyrhaug and C. R. Hess, *Chem. Sci.*, 2021, **12**, 7521-7532.
5. P. M. Stanley, C. Thomas, E. Thyrhaug, A. Urstoeger, M. Schuster, J. Hauer, B. Rieger, J. Warnan and R. A. Fischer, *ACS Catal.*, 2021, **11**, 871-882; E. Portenkirchner, J. Gasiorowski, K. Oppelt, S. Schlager, C. Schwarzinger, H. Neugebauer, G. Knör and N. S. Sariciftci, *ChemCatChem*, 2013, **5**, 1790-1796.
6. Z. K. Lopez-Castillo, S. N. V. K. Aki, M. A. Stadtherr and J. F. Brennecke, *Ind. Eng. Chem. Res.*, 2006, **45**, 5351-5360; E. Brunner, *J. CHem. Eng. Data*, 1985, **30**, 269-273.
7. U. Megerle, R. Lechner, B. König and E. Riedle, *Photochem. Photobiol.Sci.*, 2010, **9**, 1400-1406; H. Volfova, Q. Hu and E. Riedle, *EPA Newsletter*, 2019, 51-69.
8. M. Grübel, I. Bosque, P. J. Altmann, T. Bach and C. R. Hess, *Chem. Sci.*, 2018, **9**, 3313-3317; H. S. Stark, P. J. Altmann, S. Sproules and C. R. Hess, *Inorg. Chem.*, 2018, **57**, 6401-6409.
9. v. APEX suite of crystallographic software.
10. v. a. SAINT, SADBS, version 2008.1.
11. G. M. Sheldrick, *Acta Crystallogr., Sect. A: Found. Adv.*, 2015, **71**, 3-8.
12. G. M. Sheldrick, *Acta Crystallogr., Sect. C: Struct. Chem.*, 2015, **71**, 3-8.
13. C. B. Hubschle, G. M. Sheldrick and B. Dittrich, *J. Appl. Crystallogr.*, 2011, **44**, 1281-1284.
14. A. J. Wilson, *International Tables for Crystallography,*, Kluwer Academic Publishers, Dordrecht, The Netherlands, 1992.
15. A. L. Spek, *Acta Crystallogr., Sect. C: Struct. Chem.*, 2015, **71**, 9-18.
16. C. F. Macrae, P. R. Edigngton, P. McCabe, E. Pidcock, G. P. Shields, R. Taylor, M. Towler and J. v. d. Streek, *J. Appl. Crystallogr.*, 2006, **39**, 453-457.
17. J. C. Craig, N. N. Ekwuribe, C. C. Fu and K. A. M. Walker, *Synthesis*, 1981, 303-305.
18. I.-S. H. Lee, E. H. Jeoung and M. M. Kreevoy, *J. Am. Chem. Soc.*, 1997, **119**, 2722-2728.
19. E. Müller, G. Bernardinelli and A. v. Zelewsky, *Inorg. Chem.*, 1988, **27**, 4645-4651.
20. P. Banerjee, A. Company, T. Weyhermüller, E. Bill and C. R. Hess, *Inorg. Chem.*, 2009, **48**, 2944-2955.
21. K. Rickmeyer, L. Niederegger, M. Keilwerth and C. R. Hess, *ACS Catal.*, 2022, **12**, 3046-3057.